ARTICLE IN PRESS

npj Precision Oncology

https://doi.org/10.1038/s41698-026-01387-0

Article in Press

Neoadjuvant mFOLFOX6 plus camrelizumab and apatinib in colon cancer and biomarker research via spatiotemporal-omics profiling

Received: 21 July 2025

Accepted: 16 March 2026

Cite this article as: Tong, Z., Gao, L., Wang, D. *et al.* Neoadjuvant mFOLFOX6 plus camrelizumab and apatinib in colon cancer and biomarker research via spatiotemporal-omics profiling. *npj Precis. Onc.* (2026). https://doi.org/10.1038/s41698-026-01387-0

Zhou Tong, Liaoliao Gao, Danyang Wang, Peng Zhao, Xuanwen Bao, Hangyu Zhang, Xiaomeng Dai, Lulu Liu, Xudong Zhu, Yang Gao, Yi Zheng, Qihan Fu, Fanlong Liu, Wenbin Chen, Xiangming Xu & Weijia Fang

We are providing an unedited version of this manuscript to give early access to its findings. Before final publication, the manuscript will undergo further editing. Please note there may be errors present which affect the content, and all legal disclaimers apply.

If this paper is publishing under a Transparent Peer Review model then Peer Review reports will publish with the final article.

ARTICLE IN PRESS

© The Author(s) 2026. **Open Access** This article is licensed under a Creative Commons Attribution-NonCommercial-NoDerivatives 4.0 International License, which permits any non-commercial use, sharing, distribution and reproduction in any medium or format, as long as you give appropriate credit to the original author(s) and the source, provide a link to the Creative Commons licence, and indicate if you modified the licensed material. You do not have permission under this licence to share adapted material derived from this article or parts of it. The images or other third party material in this article are included in the article's Creative Commons licence, unless indicated otherwise in a credit line to the material. If material is not included in the article's Creative Commons licence and your intended use is not permitted by statutory regulation or exceeds the permitted use, you will need to obtain permission directly from the copyright holder. To view a copy of this licence, visit http://creativecommons.org/licenses/by-nc-nd/4.0/.

ARTICLE IN PRESS

Neoadjuvant mFOLFOX6 plus camrelizumab and apatinib in colon cancer and biomarker research via spatiotemporal-omics profiling

Zhou Tong[a,1], Liaoliao Gao[b,1], Danyang Wang[c,1], Peng Zhao[a,d,1], Xuanwen Bao[a,d], Hangyu Zhang[a], Xiaomeng Dai[a,d], Lulu Liu [a], Xudong Zhu[a], Yang Gao[a], Yi Zheng[a], Qihan Fu[a], Fanlong Liu [c*], Wenbin Chen[c*], Xiangming Xu[e*], Weijia Fang[a,d,f*]

a Department of Medical Oncology, The First Affiliated Hospital, Zhejiang University School of Medicine, Hangzhou, 310003, China
b School of medicine, Zhejiang University, Hangzhou, 310027, China.
c Department of colorectal surgery, The First Affiliated Hospital, Zhejiang University School of Medicine, Hangzhou, 310003, China
d State Key Laboratory (SKL) of Advanced Drug Delivery and Release Systems, Zhejiang University, Hangzhou, 310058, China
e Department of Colorectal Surgery and Oncology, The Second Affiliated Hospital, Zhejiang University School of Medicine, Hangzhou, 310000, China
f Zhejiang Provincial Key Laboratory for Drug Evaluation and Clinical Research, Hangzhou, 310003, China.

First author: Zhou Tong, MD, Department of Medical Oncology, The First Affiliated Hospital, Zhejiang University School of Medicine, Hangzhou, 310003, China. E-mail address: zju_tz@zju.edu.cn
Co-author: Liaoliao Gao, Bachelor, School of medicine, Zhejiang University, Hangzhou, 310027, China. E-mail address: liaoliao_gao@zju.edu.cn
Co-author: Danyang Wang, MD, Department of colorectal surgery, The First Affiliated Hospital, Zhejiang University School of Medicine, Hangzhou, 310003, China. E-mail address: wdy_1019@zju.edu.cn
Co-author: Peng Zhao, PhD, Department of Medical Oncology, The First Affiliated Hospital, Zhejiang University School of Medicine, Qingchun Road 79th, Hangzhou, 310003, China. E-mail address: zhaop@zju.edu.cn
Co-author: Xuanwen Bao, MD, PhD, Department of Medical Oncology, The First Affiliated Hospital, Zhejiang University School of Medicine, Hangzhou, 310003, China. E-mail address: xuanwen.bao@zju.edu.cn
Co-author: Hangyu Zhang, Master, Department of Medical Oncology, The First Affiliated Hospital, Zhejiang University School of Medicine, Hangzhou, 310003, China. E-mail address: zhanghangyu@zju.edu.cn
Co-author: Xiaomeng Dai, MD, PhD, Department of Medical Oncology, The First Affiliated Hospital, Zhejiang University School of Medicine, Hangzhou, 310003, China. E-mail address: dxm1106@zju.edu.cn
Co-author: Lulu Liu, MD, PhD, Department of Medical Oncology, The First Affiliated Hospital, Zhejiang University School of Medicine, Hangzhou, 310003, China. E-mail address: liululu2001@zju.edu.cn
Co-author: Xudong Zhu, Master, Department of Medical Oncology, The First Affiliated Hospital, Zhejiang University School of Medicine, Hangzhou, 310003, China. E-mail address: xudongzhu@zju.edu.cn
Co-author: Yang Gao, MD, Department of Medical Oncology, The First Affiliated Hospital, Zhejiang University School of Medicine, Hangzhou, 310003, China. E-mail address: gaoyang954@zju.edu.cn
Co-author: Yi Zheng, MD, Department of Medical Oncology, The First Affiliated Hospital, Zhejiang University School of Medicine, Hangzhou, 310003, China. E-mail address: oncologist@zju.edu.cn

ARTICLE IN PRESS

Co-author: Qihan Fu, MD, Department of Medical Oncology, The First Affiliated Hospital, Zhejiang University School of Medicine, Qingchun Road 79th, Hangzhou, 310003, China. E-mail address: fuqh@zju.edu.cn

***Co-Corresponding Author:** Fanlong Liu, MD, Department of colorectal surgery, The First Affiliated Hospital, Zhejiang University School of Medicine, Hangzhou, 310003, China. E-mail address: fanlong_liu@zju.edu.cn

***Co-Corresponding Author:** Wenbin Chen, MD, Department of colorectal surgery, The First Affiliated Hospital, Zhejiang University School of Medicine, Hangzhou, 310003, China.E-mail address: wenbinchen@zju.edu.cn

***Co-Corresponding Author:** Xiangming Xu, MD, Department of Colorectal Surgery and Oncology, The Second Affiliated Hospital, Zhejiang University School of Medicine, Hangzhou, 310000, China. E-mail address: xuxiangming@zju.edu.cn

***Corresponding Author:** Weijia Fang, MD, Department of Medical Oncology, The First Affiliated Hospital, Zhejiang University School of Medicine, Hangzhou, 310003, China. State Key Laboratory (SKL) of Advanced Drug Delivery and Release Systems, Zhejiang University, Hangzhou 310058, China. Zhejiang Provincial Key Laboratory for Drug Evaluation and Clinical Research, Hangzhou, 310003, China. E-mail address: weijiafang@zju.edu.cn

1 These authors contributed equally to this work

[*] These authors were corresponding authors. They contributed equally to this work.

The Lead Contact author: Weijia Fang, E-mail address: weijiafang@zju.edu.cn

ARTICLE IN PRESS

ARTICLE IN PRESS

Abstract

This is a single-arm, phase II clinical trial aimed to evaluate mFOLFOX6 plus camrelizumab and apatinib as a neoadjuvant regimen for locally advanced colon cancer. This trial was registered on ClinicalTrials.gov (NCT04625803), with the registration date of November 30, 2020. The primary endpoint was the pathological response rate (TRG 2-4, Dworak criteria). Time-of-flight, imaging mass cytometry and spatial proteomic analysis was applied to explore efficacy-related predictive biomarkers. Of 12 enrolled patients, 11 underwent surgery. The TRG 2-4 rate was 81.8% overall (87.5% in the MSS subgroup). Five patients (45.5%) achieved pathological complete response (pCR). With a median follow-up of 36.60 months, only one patient relapsed. An increase in the frequency of CD8+ T-cells and a decreased frequency of tissue-resident memory 1 (Trm-1) and regulatory T (Treg) cells are associated with a favorable response to neoadjuvant therapy. Spatiotemporal multiomics analysis highlighted tissue-resident macrophages as potential predictive biomarkers and warrants further verification.

Keyword neoadjuvant therapy, locally advanced colon cancer, immunotherapy, multi-omics analysis

ARTICLE IN PRESS

ARTICLE IN PRESS

Introduction

Colorectal cancer (CRC) is the third most common cancer globally and the second leading cause of cancer-related death(1). Despite the advantages of adjuvant chemotherapy(2), 20-30% of patients still experience recurrence(3). Regarding other GI cancers, clinical studies have confirmed that preoperative neoadjuvant therapy can improve patient overall survival(4, 5). Neoadjuvant therapy can shrink tumors and reduce the likelihood of tumor cell shedding during surgery and incomplete resection(5, 6). In addition, preoperative therapy has the potential advantage of minimizing the invasiveness of the procedure, allowing patients to recover from normal activities earlier.

Few phase III trials of preoperative therapy have been published, although the current National Comprehensive Cancer Network (NCCN) guidelines recommend neoadjuvant chemotherapy (NAC) as an option for bulky T4b tumors(7). The FOxTROT trial revealed that six weeks of preoperative oxaliplatin–fluoropyrimidine chemotherapy for operable colon cancer resulted in marked histopathologic downstaging, fewer incomplete resections, and better two-year disease control(8). The NeoCol trial demonstrated a greater proportion of R0 resection and tumor downstaging in the NAC group than in the operation group, but the study did not meet its primary endpoint, showing similar two-year disease-free survival (DFS) and overall survival (OS) rates(9). The phase III OPTICAL study revealed that NAC using mFOLFOX6 or CAPOX resulted in substantial pathologic downstaging but still did not significantly improve DFS(10). Thus, notwithstanding these perceived benefits of NAC, there remains controversy regarding the impact of NAC on improving survival (11-13), and the clinical outcomes of patients receiving perioperative chemotherapy need further improvement.

There is increasing evidence supporting the efficacy of immune checkpoint inhibitors (ICIs) in treating mismatch repair-deficient or microsatellite instability-high CRCs. The Phase III KEYNOTE-177 trial demonstrated the efficacy of anti-PD-1 therapy as the standard first-line treatment for mismatch repair-deficient metastatic colorectal cancer (14). The NICHE-2(15) and PICC trials(16) both revealed that the use of immunotherapy alone in locally advanced microsatellite instability-high (MSI-H) CRC patients can achieve a pathological complete response (pCR) of over 60%. Moreover, the combination of anti-PD-1 therapy and antiangiogenic drugs has shown promising efficacy in liver cancer(17) and renal cell carcinoma (RCC) patients(18). In the salvage line of advanced CRC, the combination of antiangiogenic drugs and immunotherapy has also shown potential advantages(19, 20). Camrelizumab is a humanized IgG4 monoclonal antibody with high affinity for PD-1. Apatinib is a highly selective VEGFR2-targeted TKI. The combination of these two drugs has shown encouraging antitumor activity in gastric or gastroesophageal junction cancer and liver cancer patients(21, 22). Preclinical studies have shown that apatinib can increase the efficacy of anti-PD-1 antibody therapy in patients with CRC by increasing PD-L1 expression(23). Additionally, it has both antitumor and antiangiogenic effects, while mitigating TME immunosuppression(24) and blocking VEGFR2 can increase the efficacy of anti-PD-1 therapy(25). The strategic combination of these agents aims to increase the response rate and efficacy of neoadjuvant therapy.

We initiated a phase II trial (NCT04625803) to investigate the efficacy and safety of the combination of camrelizumab and apatinib in addition to chemotherapy for patients with locally advanced CRC. Accumulating evidence has indicated that the tumor immune microenvironment (TIME) is associated with the efficacy of ICIs in several types of cancer(26-28). Through cytometry by time-of-flight (CyTOF), imaging mass cytometry (IMC) and spatial proteomic analysis, we investigated the association of the quantitative immune composition of the TIME with the response to the combination of neoadjuvant treatments, providing deeper insight into the host

ARTICLE IN PRESS

immune system and revealing potential therapeutic targets.

Results

Patient characteristics

From January 2021 to September 2022, owing to slow patient recruitment in our single center, only 12 patients were enrolled (**Figure 1B**). Baseline characteristics are shown in **Supplementary Table 1**. Most (10/12 [83.3%]) patients were women. There were ten patients (6 pMMR and 4 dMMR) with right-sided colon cancer. 50% (2/4) of patients with dMMR tumors and 62.5% (5/8) with pMMR tumors had clinical T4 disease, and all patients had positive lymph nodes on baseline radiographic assessment. Ten (10/12 [83.3%]) patients completed the planned cycles of neoadjuvant therapy. One patient received 3 cycles of neoadjuvant therapy due to a serious adverse event, and one patient received 2 cycles of neoadjuvant therapy for tumor perforation (**Supplementary Table 2**). Among the 12 patients, 11 underwent surgery. One patient declined surgery because of a persistent partial response and concerned about surgical risks. (surgical details are provided in **Supplementary Table 3**).

Efficacy Outcomes

The data cutoff for surveillance was March 23, 2025. The median follow-up time was 36.60 months (31.3–51.30 months).

One patient (who refused surgery) was excluded from the efficacy analysis. Among the 11 patients, TRG 2-4 rate were observed in 81.8% (9/11) of the patients overall and the pCR rate were 45.5% (5/11) overall. Among dMMR patients, 1 had grade 4 tumor regression, 1 had grade 3, and 0 had grade 2, the TRG 2-4 rate was 66.7% (2/3), and a pCR was achieved in 33.3% (1/3). Among pMMR patients, 4 had grade 4 tumor regression, 2 had grade 3, and 1 had grade 2, the TRG 2-4 rate was 87.5% (7/8), with a pCR rate of 50.0% (4/8) (**Figure 1D**). **Figure 1E** shows radiological images and gross specimens from 5 patients who achieved pCR. Nine patients (9/11[81.8%]) achieved N0. R0 resection was achieved in 100% of patients who underwent surgery. At the data cutoff, one patient experienced disease recurrence, and all patients were alive. The 2-year EFS and OS rates were 100% (**Figure 1C**). The details of the pathological response data are shown in **Table 1**.

A post hoc analysis of the clinical response was performed. In dMMR patients, cCR was observed in 12.5% (1/4) patients, cPR was was observed in 50.0% (2/4) patients, cSD was observed in 12.5% (1/4) patients. In pMMR patients, cCR was observed in 12.5% (1/8) patients, cPR was observed in 75.0% (6/8) patients, cSD was observed in 12.5% (1/8) patients. No patients had progressive disease in the neoadjuvant phase (**Figure 1D**).

Safety

Grade ≥3 treatment-related adverse events (TRAEs) were observed in 83.3% of patients. The most frequent grade 3-4 toxicities included neutropenia (10/12[83.3%]), leukopenia (4/12[33.3%]), thrombocytopenia (2/12[16.7%]), hypertension (2/12[16.7%]), and elevated alanine aminotransferase (ALT) (2/12[16.7%]), all of which resolved following treatment discontinuation or dose modification. All participants were affected by TRAEs of some grade, with the predominant manifestations being neutropenia (10/12[83.3%]), leukopenia (8/12[66.7%]), thrombocytopenia (8/12[66.7%]), and reactive cutaneous capillary endothelial proliferation (RCCEP) (8/12[66.7%]). Following appropriate dose adjustments and treatment discontinuation, no grade ≥3 AEs were observed postoperatively, and preoperative toxicity did not substantially impact surgical outcomes. Postoperatively, no complications were noted (detail provided in **Supplementary Table 3**). No treatment-related

ARTICLE IN PRESS

mortality occurred throughout the study period. Notably, the majority of grade ≥3 AEs were attributed to chemotherapy (**Table 2**).

Tumor microenvironment remodeling after neoadjuvant therapy

To explore associations between the tumor microenvironment and treatment efficacy, we performed CyTOF analysis. Freshly resected tissue samples from 10 patients at baseline and surgical specimens collected after neoadjuvant therapy (5 pCR patients and 5 nonpCR patients, 20 samples total) were collected. The details of the samples acquired for examination are shown in **Supplementary Table 4**. Samples were labeled as p-before (baseline samples for pCR patients), p-after (samples postneoadjuvant therapy for pCR patients), n-before (baseline samples for nonpCR patients) or n-after (samples postneoadjuvant therapy for nonpCR patients).

To depict the detailed immune landscape across tissues, on the basis of the expression of 41 immune markers, immune cells were divided into 11 main clusters, including $CD4^+$ T-cells, $CD8^+$ T-cells, double-negative T (DNT) cells, gdT (γδT) cells, B-cells, NK cells, macrophages, plasmacytoid dendritic cells (pDCs), neutrophils, eosinophils and basophils (**Figure 2A-2C**). After the administration of neoadjuvant therapy, the immune cells exhibited a distinct temporal distribution in the TME. The frequencies of $CD8^+$ T-cells, $CD4^+$ T-cells, and macrophages fluctuated during neoadjuvant treatment (**Figure 2D**). By comparing pretreatment and posttreatment samples, we observed that the frequencies of $CD8^+$ T-cells and DNT cells increased significantly in the pCR patients ($p=0.018$ for $CD8^+$ T-cells, $p=0.005$ for DNT cells). The frequency of $CD4^+$ T-cells also increased, but the difference was only significant in nonpCR patients ($p=0.003$). After neoadjuvant therapy, the frequencies of macrophages and neutrophils decreased significantly in pCR and nonpCR patients, respectively ($p=0.010$). The frequency of basophils decreased in pCR patients ($p=0.043$) but increased in nonpCR patients (**Figure 2E**). These data suggest that immune cells are remodeled in the TIME due to neoadjuvant therapy. A comparison of baseline samples from pCR patients and nonpCR patients revealed that the frequencies of macrophages and basophils were significantly greater in pCR patients (**Figure 2E**), whereas the frequencies of other types of cells were similar. This finding suggests that different baseline immune microenvironments may have contributed to different treatment outcomes.

The infiltration of $CD8^+$ T-cells is associated with the prognoses of patients with CRC(29). We next focused on the $CD8^+$ T-cell clusters, which were further categorized into central memory T-cells, tissue resident memory 1 (Trm-1) cells, tissue resident memory 2 (Trm-2) cells, naïve T-cells and effector memory T-cells (**Figure 3A, 3C, and Supplementary Table 5**). Trajectory analysis suggested distinct developmental trajectories of $CD8^+$ T-cell subsets, starting with naïve T-cells developing into central memory T-cells and effector memory T-cells. The developmental trajectories of Trm-1 and Trm-2 cells ultimately diverge in two different directions (**Figure 3B**). The Trm-1 subset is highly activated, expresses granzymes (GzmB) and coexpresses exhaustion markers such as PD-1 and T-bet, progressing toward exhaustion. Simultaneously, the Trm-2 subset exhibited low cytotoxicity and low proliferative capacity. After neoadjuvant therapy, the frequencies of central memory T-cells and Trm-1 cells decreased significantly in patients who achieved pCR ($p=0.03$ for central memory T-cells, $p<0.0001$ for Trm-1 cells). Frequencies of naïve T-cells and Trm-2 cells increased significantly in pCR patients ($p=0.047$ for naïve T-cells and $p=0.02$ for Trm-2 cells) (**Figure 3D**). The frequency of effector memory T-cells tended to increase in both groups. The remodeling of $CD8^+$ T-cell subsets was evident after neoadjuvant therapy, especially in patients who achieved pCR. Similarly, among the 8 subsets of $CD4^+$ T-cells, the frequency of regulatory T-cells (Tregs) among $CD4^+$ T-cells was significantly decreased after treatment in patients who achieved pCR

ARTICLE IN PRESS

(**Supplementary Table 6, Supplementary figure 1A-D**). These findings suggest that an increase in the frequency of $CD8^+$ T-cells and a decrease in the frequency of the Trm-1 and Treg subsets are associated with a favorable response to neoadjuvant therapy.

According to clustering analysis results, the macrophages were divided into 5 subsets. The frequencies of the macrophage subsets did not significantly change (**Supplementary figure 2A-D**). However, the proportion of macrophages to total immune cells significantly decreased after therapy in patients who achieved pCR (as shown in **Figure 2E**), suggesting that the role of macrophages in immunotherapy is highly complex and requires further analysis.

Peripheral blood samples from 11 patients (5 pCR patients and 6 nonpCR patients, 22 samples) were also collected at baseline and after the end of neoadjuvant therapy for analysis. Twelve clusters were identified based on 41 markers, including B-cells, eosinophils, $CD4^+$ T-cells, $CD8^+$ T-cells, conventional dendritic cells (cDCs), pDCs, innate lymphoid cells (ILCs), γδ T-cells, DNTs, double-positive T-cells (DPTs), monocytes, and natural killer (NK) cells. After neoadjuvant therapy, besides a reduction in the frequency of peripheral blood ILCs, which was only significant in the nonpCR group, the frequency changes in the remaining clusters were not significant (**Supplementary figure 3A-D**).

In this part of our study, we utilized CyTOF to profile the global immune census of TMEs following treatment. We observed a significant post-treatment increase in $CD8^+$ T cells within pCR group, suggesting that the triplet regimen may effectively convert an immunologically "cold" TME into a "hot" one.

This finding offers a partial explanation for the high response rate achieved by the regimen. However, the underlying mechanism for the different $CD8^+$ T cell dynamics in patients receiving the same treatment remained unclear. Given that baseline $CD8^+$ T cell levels showed no significant difference between groups whereas macrophage populations did (Figure2E), we hypothesized that the differential $CD8^+$ T cell response might not be due to their initial abundance, but rather influenced by other cellular components in the TME—particularly macrophages.

IMC reveals the spatial features of pretreatment TME topology related to pathological response to neoadjuvant therapy

To test this hypothesis, we then performed IMC analysis on baseline specimens, which provided spatial relationships to identify cell-cell interactions, to identify immune cell subsets that might regulate $CD8^+$ T cell activity. Besides, we hoped to identify predictive biomarkers from baseline samples to help select patients most likely to benefit from this triplet regimen. A total of 10 FFPE baseline colonoscopy patient samples (3 dMMR and 7 pMMR) were selected for IMC analysis incorporated more macrophage-related markers in the panel design (**Figure 4A**). Six patients did not achieve pCR after neoadjuvant therapy and were classified into the nonpCR group, whereas 4 patients achieved pCR and were categorized into the pCR group. A 38-marker panel (**Supplementary figure 4**) was used to explore the spatial distribution of immune cells across these 10 samples, with 19 regions of interest (ROIs). Through IMC analysis, the indicated markers were separately recognized by the metal-labeled antibodies with high specificity (**Figure 4B**), and the spatial distribution of representative cell subsets was consistent with the hematoxylin and eosin (H&E) staining images (**Supplementary figure 5A**).

The IMC images were then segmented into 169346 cells, which were grouped into 28 distinct cell clusters and annotated based on the expression of canonical markers, encompassing epithelial cells, endothelial cells, collagen I cells, immune cells, and others. (**Figure 4C, D; Supplementary figure 6).** A spatial cell map of each

ARTICLE IN PRESS

ROI was generated by mapping individual cell clusters back to their original locations **(Supplementary figure 5B)**. **Figure 4E** shows the distribution of different clusters in each sample (8 ROIs in the pCR group and 11 ROIs in the nonpCR group). Epithelial cells, M2-like macrophages, and collagen$^+$ cells constitute a large proportion of the overall spatial cell atlas (**Figure 4F**). To investigate the attributes of patients who exhibit an excellent treatment response, namely, pCR, we compared the frequency of each cell type cluster between pCR patients and nonpCR patients. We observed that the tissue-resident macrophage (resMAC) ratio in the pCR group was lower than that in the nonpCR group ($p=0.029$). However, we did not identify significant differences in the percentages of other subgroups between the pCR and nonpCR groups. These findings suggest that a reduced presence of resMACs in the tumor microenvironment may indicate a favorable clinical prognosis for patients receiving neoadjuvant therapy (**Figure 4G**).

Consistent with reports in other studies, dMMR patients exhibited increased infiltration of immune cells (**Supplementary figure 7**). In the dMMR group (3 samples, 6 ROIs), the baseline tissue presented lower levels of M2 cells, NK cells, Ki67$^+$CD8$^+$ T-cells, TIM3$^+$PD1$^+$CD103$^+$ CD8$^+$ memory T-cells, and higher levels of central CD4$^+$ memory T-cell subgroups in the pCR group than in the nonpCR group ($p<0.05$) (**Supplementary figure 8A**). In the pMMR subgroup (7 samples, 13 ROIs), only resMAC levels were lower in the pCR group than in the nonpCR group ($p<0.05$) (**Supplementary figure 8B**).

Correlation of pretreatment immune cell interactions with distinct clinical trial outcomes

To explore the mechanisms underlying the TME, a regional correlation analysis was performed to distinguish spatial interaction and avoidance pairs. In the nonpCR group, resMACs interacted more frequently with GZMB$^+$CD4$^+$ T-cells, Tregs, and memory CD8$^+$ T-cells than in the pCR group. M2-like macrophages interacted more frequently with CD15$^+$ tumor epithelial cells in the nonpCR group (**Figure 5A**). Distinct interaction and avoidance patterns were observed between resMACs and CD8$^+$ T-cells in pCR and nonpCR patients. There was a greater interaction between resMACs and CD8$^+$ T-cells in nonpCR patients **(Figure 5B)**.

Immune cell communication and interactions in the TIME are vital. Thus, the cell neighborhood (CN), defined by the nearest 20 cells to the center cell, was used to analyze and reveal multicellular structures in each ROI (**Figure 5C**). The distribution of each CN across different patients is illustrated in **Supplementary figure 9.** A total of 15 CNs were identified and annotated on the basis of major cell types, including NK-cell-enriched CN2, collagen-enriched CN3, B-cell-enriched CN5, TNF-α$^+$CD8$^+$ T-cell-enriched CN6, M2 and CD38$^+$CD4$^+$ T-cell-enriched CN8, and ResMac-enriched CN11 (**Figure 5D**). We subsequently compared the enrichment levels of each CN between the pCR and nonpCR groups. A decreasing trend in resMAC-enriched CN11 was observed in the pCR group compared with the nonpCR group, although the difference was not statistically significant (**Figure 5E**). These findings indicate that the conformation of CN11 enriched with resMACs may be associated with an unfavorable prognosis.

There may be a potential link between tumor-associated macrophages (TAMs) and exhausted CD8$^+$ T-cells, as revealed by other studies(27, 30, 31). Combined with the above findings, we next examined the ratio of immune cells to all cells around resMACs. In the nonpCR group, the frequency of TIM3$^+$PD-1$^+$CD103$^+$CD8$^+$ T-cells with exhaustion marker expression surrounding resMACs was greater than that in the pCR group, indicating that the resMACs in the nonpCR group may contribute to more T-cell exhaustion than those in the pCR group **(Figure 5F)**. These findings suggest that a lower frequency of exhausted T-cells leads to better clinical outcomes.

We next analyzed the expression of different immune cell markers around resMACs. The expression of an

ARTICLE IN PRESS

effector marker (granzyme B) in immune cells around the resMACs was not significantly different between the pCR patients and the nonpCR patients. Exhaustion-related markers such as TIM-3 in memory $CD8^+$ T-cells and PD-L1 in central memory $CD4^+$ T-cells, $GZMB^+CD4^+$ T-cells and $TIM3^+PD\text{-}1^+CD103^+CD8^+$ T-cells were increased in the nonpCR group. These findings suggest that in the nonpCR group, resMACs may lead to exhaustion of some $CD4^+$ and $CD8^+$ T-cell subsets, thus hindering the therapeutic effect **(Figure 5G)**.

The IMC results revealed that resMACs were enriched in the non-pCR group and spatially interacted with T cells, potentially driving the exhaustion of cytotoxic T cells. Together, the cyTOF and IMC results uncovered the role of resMACs in regulating the immune TME and predicting treatment outcome, providing a cellular-level explanation for the differential treatment responses.

Spatial proteomics analysis reveals distinct underlying biological mechanisms with different clinical trial outcomes

To further investigate the molecular-level mechanisms, we conducted the spatial proteomics on tumor regions identified with IMC. This approach integrates manual tissue microdissection, which improves spatial resolution through tissue expansion, with bottom-up MS-based proteomic analysis(32). This methodology includes the sequential slicing of tissue samples and the subsequent application of both IMC and proteomic analysis to explore the underlying biological mechanisms within the ROIs identified by IMC.

Initially, we examined the signaling pathways of all 19 ROIs using ssGSEA. Unsupervised analysis of immunotherapy-related, metabolic, and hallmark pathways revealed substantial intratumoral heterogeneity between baseline samples from patients who achieved pCR and those from patients who did not achieve pCR after treatment, underscoring both patient-specific and condition-specific diversity (**Figure 6A**). We then correlated the cell frequencies of the identified components via IMC with the ssGSEA scores of the pathways to assess the contributions of different cell types. For example, compared with common epithelial cells, $CD15^+$ epithelial cells presented a distinct correlation pattern, including a negative correlation with multiple metabolic pathways, whereas common epithelial cells presented the opposite trend. Among the macrophage subtypes, M2 macrophages were positively correlated with the KRAS signaling, angiogenesis, and complement pathways, whereas resMACs were negatively correlated with thiamine metabolism and the G2M checkpoint (**Figure 6E**).

To further investigate the molecular patterns contributing to different clinical outcomes, we conducted an analysis of differentially expressed proteins (DEPs) between nonpCR and pCR patient baseline samples. Notably, expression of proteins such as MAPT and HLA-E was upregulated in pCR patients, whereas that of TP53, HLA-DRB5, and IGKV6D-41 was downregulated (**Figure 6B)**. Leveraging the DEPs, we performed Gene Ontology (GO) analysis, which revealed enriched biological processes, including antigen processing, positive regulation of T-cell activation, and positive regulation of tumor necrosis factor production, in the pCR samples. Conversely, processes such as proline metabolism, glycogen catabolism, and the regulation of lipoprotein metabolism were enriched in nonpCR samples **(Figure 6C**). We then performed protein–protein interaction (PPI) network analysis using the STRING database to separately predict associations between proteins with upregulated and downregulated expression, followed by the extraction of subnetworks or neighborhoods on the basis of edge betweenness. The proteins with upregulated expression were categorized into 7 communities, whereas the proteins with downregulated expression were divided into 12 communities. Pathway enrichment analysis revealed that each community exhibited a distinct pattern. These findings highlight the molecular differences between the baseline samples of patients who achieved pCR and those who did not following neoadjuvant therapy **(Figure 6D**). These results thereby enriching our understanding of the molecular mechanisms associated

ARTICLE IN PRESS

with treatment response and providing preliminary insights into the relevant functional pathways.

In summary, our study began with a promising clinical trial and investigated the mechanism underlying different treatment response through multi-omics. CyTOF, IMC, and spatial proteomics were applied step by step, from systemic immune profiling to spatial cellular interactions and functional pathway analysis.

Discussion

In patients with locally advanced colon cancer, neoadjuvant chemotherapy results in pathologic downstaging but does not improve the DFS of patients(9, 10). Thus, a more intensive treatment approach was attempted in hopes of achieving greater tumor regression and disease control duration. Ongoing clinical trials are exploring combinations of chemotherapy and immunotherapy (NCT03985891, NCT05202314, and NCT05914389). To our knowledge, this is the first study investigating the activity of a combined regimen of chemotherapy, PD-1 blockade and a VEGFR inhibitor in locally advanced colon cancer. We chronologically enrolled patients according to strict inclusion and exclusion criteria. However, owing to difficulties in enrollment, only 12 patients were ultimately included. As Simon's two-stage design, our study has met the goal in its first stage with over five patients showing significant pathological response (TRG 2-4). Based on these compelling early results, we proceeded with exploratory analyses to promptly report these findings to the scientific community.

The combination regimen showed promising efficacy for both dMMR/MSI-H and pMMR/MSS patients, with a relatively high regression rate of 87.5% in the pMMR/MSS population. The achievement of a pCR by five patients (45.5%), with the majority being pMMR patients (4 cases), was encouraging and was higher than that reported in the previous FOxTROT study, which reported a pCR rate of 4%, with a major regression rate of 21%(8). With a median follow-up time of 36.60 months (range: 31.3–51.3 months), only one patient experienced disease recurrence. A significant advantage of ICIs has been established for MSI-H tumors. However, the majority of CRC cases are MSS and are intrinsically resistant to immune checkpoint inhibitors(33). dMMR or MSI-H tumors present high mutational burdens and immunogenic neoantigen loads, leading to abundant tumor infiltration by cytotoxic $CD8^+$ T lymphocytes; however, this is not the case for pMMR or MSS tumors, which present an immune desert or immune-excluded microenvironment(34-36). In our trial, most of the enrolled patients had pMMR, and surprisingly, of the five patients who achieved a pCR, four patients had pMMR. These findings provide preliminary evidence of a potential clinical benefit from the combination strategy in pMMR patients.

Using CyTOF, we profiled the immune landscape and uncovered substantial remodeling of the tumor microenvironment following treatment. We observed a dynamic shift in the tumor immune microenvironment (TME) post-treatment. This was characterized by a significant increase in cytotoxic $CD8^+$ T cells and a decreased frequency of tissue-resident memory 1 (Trm-1) and regulatory T (Treg) cells. This integrated observation implies the transformation of an immunosuppressive "cold" TME into a "hot" one. Tissue-resident memory T (Trm) cells constitute a subset of memory $CD8^+$ T (Tmem) cells and display only restricted recirculation potential(37). Studies have indicated that Trm cells coexpressing PD-1 and TIGIT within the tumor microenvironment exhibit an exhaustion phenotype, including impaired cytotoxic function(38). Other studies have shown that low frequency of $CD8^+CD103^+PD\text{-}1^+TIM3^+$ Trm cells are associated with longer survival(39). Similarly, in our study, we observed a significant decrease in the Trm-1 subset expressing exhaustion markers such as PD-1 following neoadjuvant treatment, which was significant in patients who achieved pCR. These data demonstrate striking neoadjuvant therapy-associated changes in colonic $CD8^+$ T-cells, characterized by a shift

ARTICLE IN PRESS

from the Trm-1 subset to the effector memory and Trm-2 subsets. Similarly, a study indicated a shift from Trm cells to proliferating $CD8^+$ T-cells in ICI-induced colitis(40). The observed post-treatment immune remodeling provided a mechanistic explanation for the observed benefit of combination immunotherapy, even in MSS patients. The similar patterns have been consistently observed in other clinical trials such as NICHE-1 (41) and NICOLE (42). The NICOLE trial, despite being a nivolumab monotherapy study, showed that pathological responses (including 1 pCR) have been observed in a subset of pMMR patients. Mechanistically, its report of a significant post-treatment increases in $CD8^+$ T-cell infiltration directly aligns with our finding of immune remodeling. Similarly, the NICHE-1 study not only reported responses in pMMR patients but identified $CD8^+PD\text{-}1^+$ T-cell infiltration as a key predictor, further underscoring the critical role of the T-cell compartment. In addition, novel combinations have been explored for more potent efficacy. The NEST-1 and NEST-2 studies with the novel botensilimab (BOT, anti-CTLA-4) and balstilimab (BAL, anti-PD-1) demonstrated dramatically higher pathological response rates (60% with >50% regression in NEST-2 MSS cohort) (43). This underscores that the dual checkpoint inhibitor regimen can more effectively overcome the immunosuppressive barriers in MSS tumors. The replication of these impressive results in the Italian UNICORN trial confirms the robustness and generalizability of this approach (44). Furthermore, an "inside-out" (serosa-to-mucosa) tumor regression and extensive immune infiltration is seen in the spatial biology findings, revealing mechanisms of actions of BOT (45).

Based on our findings, we propose a cohesive model for how the triplet regimen may synergize to remodel "cold" pMMR/MSS immune microenvironment. Firstly, our therapeutic regimen was built upon a foundation of oxaliplatin-based chemotherapy. Oxaliplatin contributes to anti-tumor immunity by inducing immunogenic cell death (ICD) (46)and enhancing tumor antigen presentation through upregulation of MHC-I expression(47). This process facilitates more robust T cell activation thus create a favorable context for immune checkpoint blockade. One study demonstrated FOLFOX chemotherapy reinvigorate tumor-infiltrating $CD8^+$ T cells, reversing their exhausted phenotype and promoting a transition to a functional effector state, thereby improving clinical outcomes in colorectal cancer(48). Secondly, apatinib, the anti-angiogenic agent, likely acts as a powerful "conditioner" of the TME. VEGF inhibition exerts multifaceted immunomodulatory effects, including: improved dendritic cell-mediated antigen presentation; enhanced T cell priming; normalized tumor vasculature promoting lymphocyte infiltration from lymph nodes to tumor sites. Concurrently, it suppresses immunosuppressive populations such as Tregs, TAMs, and myeloid-derived suppressor cells (MDSCs)(49). The combination therapy consistently induced the anticipated immune shifts: an increase in $CD8^+$ T cells accompanied by a reduction of Treg and macrophage infiltration. Collectively, these actions rebalance the tumor microenvironment from an immunosuppressive to an immunopermissive state. Finally, the convergence of these mechanisms, oxaliplatin-driven immunogenicity and T cell effector reprogramming combined with apatinib-mediated vascular normalization, creates a potent synergistic platform for camrelizumab, leading to treatment effectiveness. It is important to note that the synergistic mechanism described here remains a hypothesis derived from the literature and it requires further experimental investigation.

Our spatial data offer a deeper explanation of the spatial architecture underlying efficacy by IMC, which is rarely reported in previous neoadjuvant therapy studies. We discovered that at baseline, nonpCR patients were characterized by specific spatial neighborhoods featuring interaction between T cells and resMACs. ResMACs are present in most tissues and are endowed with general as well as tissue-specific functions(50). In the early stages of tumor development, resMACs accumulate near tumor cells, promoting epithelial–mesenchymal

ARTICLE IN PRESS

transition and invasiveness in tumor cells(51, 52). The abundance of resMACs has been linked to unfavorable outcomes across several types of solid tumors(53, 54), with numerous studies documenting their immunosuppressive function in progression and dissemination(55). Consistent with a previous study(56), our study revealed that resMAC are negatively correlated with the prognosis of tumors and are less enriched in patients in the pCR group. CRC patients with lower resMAC enrichment may benefit from our neoadjuvant regimen. However, a study revealed that patients with tumors harboring an increased proportion of macrophages resembling breast $TIM4^+$ perivasculature had improved survival rates(56). Despite extensive research, there are still large gaps in our comprehensive understanding of the complexity of resMACs(57, 58).Intravital imaging research has revealed the preferential localization of antigen-specific $CD8^+$ T-cells in regions abundant with TAMs within the TME, resulting in enduring close interactions(59-62). Kelly Kersten et al. reported that TAMs and exhausted T-cells (Texs) are interdependent, with Texs shaping myeloid cell recruitment and phenotype, whereas TAMs sustain the exhaustion of $CD8^+$ T-cells, both of which contribute to tumor progression(63). The expression of PD-1 in T-cells indicates the depletion characteristics of T-cells, but the role of PD-L1 in T-cell expression is controversial. Research shows that PD-$L1^+$ T-cells can play a role in tumor promotion via three distinct mechanisms(64). In our work, we observed interactions between resMACs and surrounding immune cells and noted increased expression of exhaustion markers such as PD-1, PD-L1 and TIM3 surrounding resMACs in the nonpCR group.

This finding suggests that resMAC testing could be implemented for patients with locally advanced colorectal cancer, thereby improving the selection of individuals who are most likely to respond to the current triplet regimen. On the other hand, for patients exhibiting high resMAC infiltration at baseline, this finding motivates the development of new therapeutic approaches. Combining the current regimen with targeted strategies including therapeutics designed to induce macrophage depletion, impair recruitment, and induce repolarization could potentially overcome the resistance mechanism and extend therapeutic benefit to this patient subgroup (65). By bridging this biomarker discovery to clinical strategies, we hope to provide a clearer roadmap for its future application and the personalization of therapy in this setting.

Furthermore, spatial proteomics analysis was applied to discover the molecular mechanisms involved within the ROIs identified by IMC, providing deeper insights into the functional pathways involved in treatment response. MAPT promoter CpG island hypermethylation is associated with a poor prognosis in patients with stage II CRC(66). Since CpG island hypermethylation always inhibits gene expression, high MAPT expression may predict better prognosis in CRC patients. A similar phenomenon was observed in breast cancer patients treated with adjuvant anthracycline and paclitaxel chemotherapy and endocrine therapy(67). HLA class II proteins (HLA DP, DQ, DR) have limited expression on antigen-presenting cells and present antigens to $CD4^+$ T-cells(68). Specific HLA class I alleles have been associated with ICI efficacy and toxicity(69, 70). Some studies have noted that increased HLA class II-related gene expression is correlated with improved outcomes(71). Notably, increased HLA-DR expression has been suggested to predict the ICI response(72, 73). Consistent with previous studies, our study revealed that HLA-DRB4 and HLA-E expression were upregulated in patients who achieved pCR. In addition to DEP analysis, GO analysis and PPI analysis revealed distinct enrichment in biological processes and protein associations between patients who achieved pCR and those who did not.

We report a higher incidence of grade 3 or higher thrombocytopenia and neutropenia than other neoadjuvant chemotherapy studies(10, 74). The safety profile of camrelizumab plus apatinib and FOLFOX was consistent with the known toxicities of the individual components. While the triple combination showed enhanced efficacy,

ARTICLE IN PRESS

this benefit may come at the cost of an increased rate of adverse events, a phenomenon consistently observed across similar combination clinical trials as AtezoTRIBE (75)and CheckMate 9X8 (76). The most frequent Grade ≥3 adverse events were neutropenia (83.3%), leukopenia (33.3%), and thrombocytopenia (16.7%). The incidence of hematologic events such as neutropenia (83.3%), appear elevated compared to FOLFOX chemotherapy alone(77, 78). While the FOLFOX regimen is known to cause myelosuppression, apatinib, an anti-VEGFR2 TKI also carries known side effects including thrombocytopenia, neutropenia, hypertension and fatigue (79, 80). The hematological toxicities, likely attributable to the overlapping toxicity profiles of the combined agents. In addition, two patients (16.7%) developed Grade ≥3 elevated alanine aminotransferase (ALT) are likely a consequence of overlapping hepatic toxicities from the combined agents. However, all AEs were manageable and reversible. No suspected unexpected serious adverse reactions (SUSARs) occurred, and there were no treatment-related deaths in our study. AE were managed with appropriate interventions, including granulocyte colony-stimulating factor (G-CSF) support and dose adjustments. Most patients (83.3%, 10/12) completed all planned cycles of neoadjuvant therapy (**Supplementary Table 2**). Based on our experience, we propose that the long-term feasibility of this triplet regimen in a broader population could be enhanced by several measures: (1) stricter patient selection: for example, excluding insufficient bone marrow reserve at baseline or ECOG ≥ 2; (2) routine primary prophylaxis with long-acting G-CSF to reduce the incidence of severe neutropenia; (3) close monitoring with prompt intervention upon early signs of toxicity. Future larger-scale trials incorporating these supportive strategies may be crucial to confirm its long-term feasibility.

While promising clinical effects and potential biomarkers have been obtained from our study, there are several limitations. First, the study is limited by its small sample size and an imbalance in tumor location and gender. Second, our study was a single-arm phase II clinical trial, which lacked the control group. A high pCR rate and encouraging DFS and OS outcomes require validation in larger, randomized trials with expanded cohorts. Third, a notably high incidence of adverse events within this relatively small sample size was observed. At last, through multiomics analysis, we investigated efficacy-related predictive biomarkers. Due to the limited sample size and primarily descriptive results, the underlying mechanism requires further exploration through in vitro and in vivo experiments.

In conclusion, the neoadjuvant regimen combining mFOLFOX6 with camrelizumab and apatinib was observed to induce a pCR rate of 45.5% in patients with locally advanced colon cancer, independent of MMR status. Potential predictive biomarkers of response may include lower baseline levels of resMAC infiltration and a posttreatment increase in $CD8^+$ T-cells. The presence of resMACs in the tumor microenvironment appeared to correlate with exhaustion in certain $CD4^+$ and $CD8^+$ T-cell subsets, which might negatively affect treatment efficacy. These findings add to the preliminary understanding of this triple-combination therapy and support further investigation into biomarker-guided strategies.

Methods

Study design and participants

This investigator-initiated, single-arm, phase 2 study was performed at the First Affiliated Hospital of Zhejiang University. Eligible patients were (1) aged 18–75 years; (2) had an Eastern Cooperative Oncology Group performance status (ECOG PS) of 0–1; (3) had histopathologically or cytologically confirmed colon adenocarcinoma without distant metastases (T4 or T3 with extramural depth ≥5 mm, N0–2, M0)(78); and (4) had adequate organ function and expected survival ≥12 months. Tumors were staged using the 8th edition of the

ARTICLE IN PRESS

American Joint Committee of Cancer (AJCC) tumor–node–metastasis (TNM) staging classification for colon cancer. Mismatch repair was determined by immunohistochemistry, and MSI status was determined by PCR. The key exclusion criteria were as follows: (1) evidence of distant metastatic disease; (2) obstruction, perforation, or bleeding requiring urgent treatment; and (3) the presence or history of an autoimmune disease or need for immunosuppressants. Following the principles of the Declaration of Helsinki, all patients provided written informed consent before study enrollment. The clinical study has been registered at ClinicalTrials.gov (NCT04625803) with the registration date of November 30, 2020. National Health Commission Medical Research Registration information system number: MR-33-20-004515. This study was approved by the Ethics Committee, and the ethics number is (2020) IIT Review No. (697).

Until November 4, 2021, the treatment regimen remained the same regardless of patient MSI status. However, after November 4, 2021, the plan was modified and approved under the ethics number (2021) IIT Review No. (867). As in the PICC study(16), anti-PD-1 therapy alone demonstrated an impressive pCR rate in patients with locally advanced MSI-H colon cancer. Thus, for MSI-H patients, chemotherapy was not administered to avoid overtreatment, and only camrelizumab plus apatinib were given.

Procedures

Patients with microsatellite-stable or proficient mismatch repair (pMMR) received 5 cycles of mFOLFOX6 and camrelizumab (200 mg intravenously on day 1, every 2 weeks) and apatinib (250 mg orally once daily, 2 months). mFOLFOX6 consisted of 85 mg/m^2 oxaliplatin on day 1, 400 mg/m^2 leucovorin on day 1, and 400 mg/m^2 fluorouracil on day 1, followed by continuous infusion of 2,400 mg/m^2 fluorouracil over 46 h, which was repeated once every 2 weeks. Surgery was scheduled within 4–6 weeks after the last cycle of therapy. Seven cycles of adjuvant camrelizumab plus mFOLFOX6 were administered after surgery. For patients with MSI-H or deficiency in mismatch repair (dMMR), 5 cycles of camrelizumab (200 mg intravenously on day 1, every 2 weeks) plus apatinib (250 mg orally once daily, 2 months) were given preoperatively, and 7 cycles of camrelizumab plus apatinib were given postoperatively. CT of the chest, abdomen, and pelvis was performed at baseline and was recommended after 5 cycles of mFOLFOX6. After surgery, imaging examinations were performed before and at the end of postoperative adjuvant chemotherapy. After all the treatments were completed, imaging examinations were scheduled once every 12 weeks and then once every six months after 1 year.

Tissue samples and peripheral blood samples were collected for further multiomics analysis. The workflow is shown in **Figure 1A**.

Outcome assessment

The primary endpoint was the pathological response rate, which was defined as the proportion of patients with a tumor regression grade (TRG) of 2-4 according to the Dworak criteria(81) for mismatch repair-proficient and microsatellite-stable (pMMR/MSS) patients.

The secondary endpoints included the tumor pathological downstaging rate, defined as the percentage of patients with a lower postoperative stage than baseline stage, the pCR rate, the R0 resection rate, 2-year DFS, 2-year EFS and OS for MSS colon cancer patients; pathology response rate and pCR rate for MSI-H/dMMR patients; and perioperative complication rates, mortality rates and adverse events (National Cancer Institute Common Terminology Criteria for Adverse Events [NCI CTCAE], version 5.0). Safety outcomes were assessed using the safety analysis set of all patients exposed to at least one dose of intervention.

ARTICLE IN PRESS

Cy-TOF data acquisition and analysis

Tumor tissues and peripheral blood samples were obtained from the patients who participated in the study for cytometry by time-of-flight (CyTOF) analysis. Tissue samples were collected during the baseline colonoscopy and surgery, whereas peripheral blood samples were taken at baseline and at the end of the neoadjuvant therapy. An immune cell-centric antibody panel that includes 41 antibodies. Single-cell suspensions were obtained through enzyme cocktail digestion as described in a previous study(82). PBMCs were obtained by Ficoll gradient centrifugation according to the manufacturer's protocol as described previously(83). The resulting single-cell suspension was first incubated with 0.25 μM cisplatin (Fluidigm, USA) for 5 min on ice to exclude dead cells. After 3 washes, the cells were resuspended and incubated with block mix buffer (Fluidigm) for 20 min on ice to block nonspecific antibody binding to Fc receptors. Then, the cells were incubated on ice with a cell-surface antibody cocktail for 30 min and washed twice with FACS buffer. Before intracellular antibody incubation, the cells were fixed with fresh 1.6% formaldehyde (FA) solution at room temperature for 10 min and then incubated with DNA Intercalator-Ir solution (Maxpar Fix and Perm Buffer containing 250 nM 191/193Ir, Fluidigm) at 4 °C overnight. Next, the cells were washed and permeabilized with Foxp3/transcription factor staining buffer (eBiosciences), followed by incubation on ice with intracellular antibodies for 30 min. The cells were then washed and resuspended in 0.1X EQ Four Element Calibration Beads and applied to a mass cytometer (Helios, Fluidigm). The data of each sample were debarcoded from the raw data using a doublet-filtering scheme with unique mass-tagged barcodes. Each FCS file generated from different batches was normalized via the bead normalization method. The data were manually gated using FlowJo software to exclude debris, dead cells, and doublets, leaving only live, single cells. The PARC clustering algorithm was applied to all cells to partition the cells into distinct phenotypes on the basis of marker expression levels. The clustering parameters were adjusted to obtain a suitable number of clusters. The cell type of each cluster was annotated according to its marker expression pattern on a heatmap of clusters vs. markers. The dimensionality reduction algorithm t-SNE was used to visualize high-dimensional data in two dimensions, displaying the distribution of each cluster, marker expression, and variations among different groups or sample types. A t test was used to analyze the frequency of the annotated cell population.

Imaging mass cytometry (IMC) analysis

Paraffin-embedded and formalin-fixed tissues were selected for IMC and downstream analysis from baseline colonoscopy biopsies from patients included in the study. Serial sectioning was performed, and one of the sections was subjected to H&E staining. The pathologist subsequently identified one or two ROIs of 1× 1 mm^2 infiltrated most abundantly with immune cells on the basis of the pathological morphological structure revealed by H&E staining. Based on our previously published study, the ROIs were defined as square areas with a laser intensity of 400 Hz(84). An imaging mass cytometer (Fluidigm, Hyperion) was used to scan the prepared sections and generate multiplexed images. The IMC data analysis pipeline consists of four steps: spillover signal compensation, image denoising, image contrast enhancement, and cell segmentation. The individual cell or component in each channel of the IMC image was segmented using the connection-sensing segmentation method(85). For cell segmentation, MATLAB function region props were applied to detect connected components in the image for cell segmentation. For other membrane channels, we eliminated artifacts if their distance to the nearest nucleus centroid was greater than 15 pixels. The expression of each marker was

ARTICLE IN PRESS

normalized to the 99th percentile for each channel. A picture clustering algorithm was adopted to complete the analysis in R 3.3.4. The cells of all the samples were mixed, and cluster analysis was performed using a master cell group marker. All the data were processed via the arcsinh transformation (cofactor set to 1) and normalized before clustering. The "imcRtools" package (version 1.0.2) was used for downstream analysis. The cell neighborhood (CN) of each cell was composed of its 20 nearest neighbors. These neighborhoods were grouped and annotated according to their cell components using K-means clustering (k=15), and the results were verified by superimposing Voronoi plots of corresponding cell neighborhoods on the original tissue IMC image. Through neighborhood analysis of cell types in different ROIs, 15 different cell neighborhood structures were constructed and clustered. A permutation test method of the "imcRtools" package (version 1.0.2) was used to evaluate the interactions/avoidances between different cell clusters to explore spatial cell–cell interactions(86). Patch detection was used to detect the local accumulation of cells of interest. A distance of 20 μm was defined as the maximum distance between cells to be considered part of the patch, and 30 was the minimal number of cells by which a patch was defined(86).

Spatial proteomics and downstream analysis

FFPE samples of colon cancer tissues at baseline were prepared into 4 μm slices. Hydrogel embedding, tissue expansion, staining, imaging, microdissection, tissue polypeptide recovery and mass spectrometry of the recovered polypeptides were performed as previously described(32). Following treatment with BT buffer and MES buffer, the slices were incubated with a protein anchoring solution for 12 h. The samples were subsequently rinsed with anchoring stop buffer, exposed to activated monomer solution in a gelation chamber at 4 °C for 12 h to induce gelation, and then moved to a vacuum oven for the polymerization reaction. The subsequent stage of expansion involved immersing the resulting tissue-hydrogel composite in a uniform buffer. Following Coomassie blue staining and repeated washing, the tissues were visualized using a Zeiss Fluorescence Stereo Zoom Microscope. Microdissection of the expanded Coomassie-stained samples was performed on the basis of the ROIs, and the samples were analyzed via liquid chromatography (LC)-mass spectrometry (MS)/MS. A hybrid trapped ion mobility spectrometry (TIMS) quadrupole time–of–flight mass spectrometer (timsTOF-Pro) was used for peptide extraction and analysis in parallel accumulation–serial fragmentation combined with data-independent acquisition parallel accumulation serial fragmentation (diaPASEF) mode, as previously described(32, 87). We used Bruker otofControl (version 6.2) and HyStar (version 5.1) for MS data acquisition. The FragPipe (version 15.0) platform and MSFragger (version 3.1.1)(88, 89) were used for DDA data analysis. The self-built library was further used to analyze PulseDIA data via DIA-NN (version 1.7.15)(90). The ssGSEA score for each gene set was calculated using the "GSVA" package in R software (version 1.50.0)(91). We performed differentially expressed protein (DEP) analysis via the "DESeq2" package (version 1.44.0)(92) and Gene Ontology (GO) analysis using the "clusterProfiler" package (version 4.10.0)(93). Protein–protein interaction (PPI) network visualization was performed in Cytoscape 3.10.1 (http://www.cytoscape.org). The correlation analysis of pathway scores and cell frequencies in the IMC data was performed via the "psych" package (version 2.4.6).

Statistical analysis

This was a single-arm study, and no randomization was used. To determine the sample size, we used the Simon 2-stage optimum design with a unilateral alpha of 0.05 to achieve a power of 0.8, and the pathological

ARTICLE IN PRESS

response rate (TRG 2-4) was expected to increase from 22.5% to 40%. Considering a 10% shedding rate, it was estimated that 64 patients needed to be enrolled.

All the statistical analyses were performed using SPSS Statistics 26 (IBM, Armonk, NY, USA). Continuous variables with parametric distributions were evaluated using t tests. Categorical variables were evaluated using the chi-square test (or Fisher's exact test where appropriate). All the statistical tests were two-sided, and the significance threshold for all the P values was 0.05. Graphs were generated using GraphPad Prism (version 10.1.1). We used the CONSORT reporting guideline(94) to draft this manuscript, and the CONSORT reporting checklist when editing, included in supplement files.

Acknowledgments

We appreciate our gratitude to Prof. Jun Li for her valuable work in pathological analysis and to Prof. Bin Qi for his role in radiological tumor evaluation. This work was supported by the National Natural Science Foundation of China (82203186, 82373428), The "Pioneer" and "Leading Goose" R&D Program of Zhejiang (2025C02073), Noncommunicable Chronic Diseases-National Science and Technology Major Project (2023ZD0501600), and Beijing Xisike Clinical Oncology Research Foundation (Y-NESTLE2022QN-0345). The funder played no role in study design, data collection, analysis, and interpretation of data, or the writing of this manuscript.

Data Availability

Data are not publicly available due to privacy requirements but are available upon reasonable request from the corresponding author.

Code Availability

Not application

Competing Interests

The authors declare no competing interests.

Authors 'contributions

Zhou Tong, Weijia Fang-literature search, study design, writing
Xuanwen Bao, Liaoliao Gao- data analysis, data interpretation
Danyang Wang, Wenbin Chen - patients enrollment
Xiaomeng Dai, Hangyu Zhang, Lulu Liu -figures, data collection
Yang Gao, Xudong Zhu- patient management and treatment
Yi Zheng, Qihan Fu- data analyses
Peng Zhao, Fanlong Liu- study design, revised the manuscript
Xiangming Xu, Weijia Fang - study design, supervised the research

ARTICLE IN PRESS

ARTICLE IN PRESS

Reference

1. Siegel RL, Giaquinto AN, Jemal A. Cancer statistics, 2024. CA Cancer J Clin. 2024;74(1):12-49.

2. André T, Boni C, Navarro M, Tabernero J, Hickish T, Topham C, et al. Improved overall survival with oxaliplatin, fluorouracil, and leucovorin as adjuvant treatment in stage II or III colon cancer in the MOSAIC trial. J Clin Oncol. 2009;27(19):3109-16.

3. André T, Boni C, Mounedji-Boudiaf L, Navarro M, Tabernero J, Hickish T, et al. Oxaliplatin, fluorouracil, and leucovorin as adjuvant treatment for colon cancer. N Engl J Med. 2004;350(23):2343-51.

4. Surgical resection with or without preoperative chemotherapy in oesophageal cancer: a randomised controlled trial. Lancet. 2002;359(9319):1727-33.

5. Cunningham D, Allum WH, Stenning SP, Thompson JN, Van de Velde CJ, Nicolson M, et al. Perioperative chemotherapy versus surgery alone for resectable gastroesophageal cancer. The New England journal of medicine. 2006;355(1):11-20.

6. Alieva M, van Rheenen J, Broekman MLD. Potential impact of invasive surgical procedures on primary tumor growth and metastasis. Clin Exp Metastasis. 2018;35(4):319-31.

7. Peng C, Kircher SM. Neoadjuvant Chemotherapy in Colon Cancer: More Than Just an Optical Illusion. J Clin Oncol. 2024;42(25):2949-54.

8. Morton D, Seymour M, Magill L, Handley K, Glasbey J, Glimelius B, et al. Preoperative Chemotherapy for Operable Colon Cancer: Mature Results of an International Randomized Controlled Trial. J Clin Oncol. 2023;41(8):1541-52.

9. Jensen LH, Kjaer ML, Larsen FO, Hollander NH, Rahr HB, Pfeffer F, et al. Phase III randomized clinical trial comparing the efficacy of neoadjuvant chemotherapy and standard treatment in patients with locally advanced colon cancer: The NeoCol trial. Journal of Clinical Oncology. 2023;41(17_suppl):LBA3503-LBA.

10. Hu H, Zhang J, Li Y, Wang X, Wang Z, Wang H, et al. Neoadjuvant Chemotherapy With Oxaliplatin and Fluoropyrimidine Versus Upfront Surgery for Locally Advanced Colon Cancer: The Randomized, Phase III OPTICAL Trial. J Clin Oncol. 2024:JCO2301889.

11. Gosavi R, Chia C, Michael M, Heriot AG, Warrier SK, Kong JC. Neoadjuvant chemotherapy in locally advanced colon cancer: a systematic review and meta-analysis. Int J Colorectal Dis. 2021;36(10):2063-70.

12. Davey MG, Amir AH, Ryan OK, Donnelly M, Donlon NE, Regan M, et al. Evaluating the oncological safety of neoadjuvant chemotherapy in locally advanced colon carcinoma: a systematic review and meta-analysis of randomised clinical trials and propensity-matched studies. Int J Colorectal Dis. 2023;38(1):193.

13. Liang Z, Li Z, Yang Q, Feng J, Xiang D, Lyu H, et al. The role of neoadjuvant chemotherapy in patients with locally advanced colon cancer: A systematic review and meta-analysis. Front Oncol. 2022;12:1024345.

14. André T, Shiu KK, Kim TW, Jensen BV, Jensen LH, Punt C, et al. Pembrolizumab in Microsatellite-Instability-High Advanced Colorectal Cancer. N Engl J Med. 2020;383(23):2207-18.

15. Chalabi M, Verschoor YL, van den Berg J, Sikorska K, Beets G, Lent AV, et al. LBA7 Neoadjuvant immune checkpoint inhibition in locally advanced MMR-deficient colon cancer: The NICHE-2 study. Annals of Oncology. 2022;33:S1389.

16. Hu H, Kang L, Zhang J, Wu Z, Wang H, Huang M, et al. Neoadjuvant PD-1 blockade with toripalimab, with or without celecoxib, in mismatch repair-deficient or microsatellite instability-high, locally advanced, colorectal cancer (PICC): a single-centre, parallel-group, non-comparative, randomised, phase 2 trial. Lancet Gastroenterol Hepatol. 2022;7(1):38-48.

ARTICLE IN PRESS

17. Xu J, Shen J, Gu S, Zhang Y, Wu L, Wu J, et al. Camrelizumab in Combination with Apatinib in Patients with Advanced Hepatocellular Carcinoma (RESCUE): A Nonrandomized, Open-label, Phase II Trial. Clin Cancer Res. 2021;27(4):1003-11.
18. Choueiri TK, Eto M, Motzer R, De Giorgi U, Buchler T, Basappa NS, et al. Lenvatinib plus pembrolizumab versus sunitinib as first-line treatment of patients with advanced renal cell carcinoma (CLEAR): extended follow-up from the phase 3, randomised, open-label study. Lancet Oncol. 2023;24(3):228-38.
19. Guo Y, Zhang W, Ying J, Zhang Y, Pan Y, Qiu W, et al. Phase 1b/2 trial of fruquintinib plus sintilimab in treating advanced solid tumours: The dose-escalation and metastatic colorectal cancer cohort in the dose-expansion phases. Eur J Cancer. 2023;181:26-37.
20. Fukuoka S, Hara H, Takahashi N, Kojima T, Kawazoe A, Asayama M, et al. Regorafenib Plus Nivolumab in Patients With Advanced Gastric or Colorectal Cancer: An Open-Label, Dose-Escalation, and Dose-Expansion Phase Ib Trial (REGONIVO, EPOC1603). J Clin Oncol. 2020;38(18):2053-61.
21. Xu J, Zhang Y, Jia R, Yue C, Chang L, Liu R, et al. Anti-PD-1 Antibody SHR-1210 Combined with Apatinib for Advanced Hepatocellular Carcinoma, Gastric, or Esophagogastric Junction Cancer: An Open-label, Dose Escalation and Expansion Study. Clin Cancer Res. 2019;25(2):515-23.
22. Li C, Tian Y, Zheng Y, Yuan F, Shi Z, Yang L, et al. Pathologic Response of Phase III Study: Perioperative Camrelizumab Plus Rivoceranib and Chemotherapy Versus Chemotherapy for Locally Advanced Gastric Cancer (DRAGON IV/CAP 05). J Clin Oncol. 2024:JCO2400795.
23. Cai X, Wei B, Li L, Chen X, Liu W, Cui J, et al. Apatinib enhanced anti-PD-1 therapy for colon cancer in mice via promoting PD-L1 expression. Int Immunopharmacol. 2020;88:106858.
24. Scott LJ. Apatinib: A Review in Advanced Gastric Cancer and Other Advanced Cancers. Drugs. 2018;78(7):747-58.
25. Li Q, Wang Y, Jia W, Deng H, Li G, Deng W, et al. Low-Dose Anti-Angiogenic Therapy Sensitizes Breast Cancer to PD-1 Blockade. Clin Cancer Res. 2020;26(7):1712-24.
26. Bortolomeazzi M, Keddar MR, Montorsi L, Acha-Sagredo A, Benedetti L, Temelkovski D, et al. Immunogenomics of Colorectal Cancer Response to Checkpoint Blockade: Analysis of the KEYNOTE 177 Trial and Validation Cohorts. Gastroenterology. 2021;161(4):1179-93.
27. Bi K, He MX, Bakouny Z, Kanodia A, Napolitano S, Wu J, et al. Tumor and immune reprogramming during immunotherapy in advanced renal cell carcinoma. Cancer Cell. 2021;39(5):649-61 e5.
28. Zhang Y, Chen H, Mo H, Hu X, Gao R, Zhao Y, et al. Single-cell analyses reveal key immune cell subsets associated with response to PD-L1 blockade in triple-negative breast cancer. Cancer Cell. 2021;39(12):1578-93 e8.
29. Galon J, Costes A, Sanchez-Cabo F, Kirilovsky A, Mlecnik B, Lagorce-Pages C, et al. Type, density, and location of immune cells within human colorectal tumors predict clinical outcome. Science (New York, NY). 2006;313(5795):1960-4.
30. Christofides A, Strauss L, Yeo A, Cao C, Charest A, Boussiotis VA. The complex role of tumor-infiltrating macrophages. Nat Immunol. 2022;23(8):1148-56.
31. Sica A, Larghi P, Mancino A, Rubino L, Porta C, Totaro MG, et al. Macrophage polarization in tumour progression. Semin Cancer Biol. 2008;18(5):349-55.
32. Li L, Sun C, Sun Y, Dong Z, Wu R, Sun X, et al. Spatially resolved proteomics via tissue expansion. Nat Commun. 2022;13(1):7242.

ARTICLE IN PRESS

ARTICLE IN PRESS

33. Le DT, Uram JN, Wang H, Bartlett BR, Kemberling H, Eyring AD, et al. PD-1 Blockade in Tumors with Mismatch-Repair Deficiency. N Engl J Med. 2015;372(26):2509-20.
34. Giannakis M, Mu XJ, Shukla SA, Qian ZR, Cohen O, Nishihara R, et al. Genomic Correlates of Immune-Cell Infiltrates in Colorectal Carcinoma. Cell Rep. 2016;17(4):1206.
35. Chen DS, Mellman I. Oncology meets immunology: the cancer-immunity cycle. Immunity. 2013;39(1):1-10.
36. Hegde PS, Karanikas V, Evers S. The Where, the When, and the How of Immune Monitoring for Cancer Immunotherapies in the Era of Checkpoint Inhibition. Clin Cancer Res. 2016;22(8):1865-74.
37. Gebhardt T, Palendira U, Tscharke DC, Bedoui S. Tissue-resident memory T cells in tissue homeostasis, persistent infection, and cancer surveillance. Immunol Rev. 2018;283(1):54-76.
38. Jiang F, Mao M, Jiang S, Jiao Y, Cao D, Xiang Y. PD-1 and TIGIT coexpressing CD8 + CD103 + tissue-resident memory cells in endometrial cancer as potential targets for immunotherapy. Int Immunopharmacol. 2024;127:111381.
39. Romagnoli G, D'Alessandris QG, Capone I, Tavilla A, Canini I, Lapenta C, et al. CD8+CD103+PD1+TIM3+ T cells in glioblastoma microenvironment correlate with prognosis. Immunology. 2024;171(2):198-211.
40. Luoma AM, Suo S, Williams HL, Sharova T, Sullivan K, Manos M, et al. Molecular Pathways of Colon Inflammation Induced by Cancer Immunotherapy. Cell. 2020;182(3):655-71 e22.
41. Chalabi M, Fanchi LF, Dijkstra KK, Van den Berg JG, Aalbers AG, Sikorska K, et al. Neoadjuvant immunotherapy leads to pathological responses in MMR-proficient and MMR-deficient early-stage colon cancers. Nat Med. 2020;26(4):566-76.
42. Avallone A, De Stefano A, Pace U, Catteau A, Di Gennaro E, Tatangelo F, et al. 491P Neoadjuvant nivolumab in early stage colorectal cancer. Annals of Oncology. 2020;31:S449.
43. Hissong E, Jafari MD, Khan S, Kasi PM, Guniganti P, Ocean AJ, et al. Neoadjuvant botensilimab (BOT) plus balstilimab (BAL) in resectable mismatch repair proficient (pMMR) and deficient (dMMR) colorectal cancer (CRC): NEST clinical trial update. Journal of Clinical Oncology. 2025;43(4_suppl):207-.
44. Ambrosini M, Raimondi A, Sabella G, Cerantola R, Palermo F, Di Donato S, et al. Preoperative botensilimab (BOT) with or without balstilimab (BAL) for patients with resectable locally advanced pMMR or dMMR colon cancer: Results from the UNICORN trial by GONO. JOURNAL OF CLINICAL ONCOLOGY. 2025;43(4_SUPPL):158-.
45. Kasi PM, Hidalgo M, Jafari MD, Yeo H, Lowenfeld L, Khan U, et al. Neoadjuvant botensilimab plus balstilimab response pattern in locally advanced mismatch repair proficient colorectal cancer. Oncogene. 2023;42(44):3252-9.
46. Tesniere A, Schlemmer F, Boige V, Kepp O, Martins I, Ghiringhelli F, et al. Immunogenic death of colon cancer cells treated with oxaliplatin. Oncogene. 2010;29(4):482-91.
47. Park SJ, Ye W, Xiao R, Silvin C, Padget M, Hodge JW, et al. Cisplatin and oxaliplatin induce similar immunogenic changes in preclinical models of head and neck cancer. Oral Oncol. 2019;95:127-35.
48. Guan Y, Kraus SG, Quaney MJ, Daniels MA, Mitchem JB, Teixeiro E. FOLFOX Chemotherapy Ameliorates CD8 T Lymphocyte Exhaustion and Enhances Checkpoint Blockade Efficacy in Colorectal Cancer. Front Oncol. 2020;10:586.
49. Kudo M. Combination Cancer Immunotherapy with Molecular Targeted Agents/Anti-CTLA-4 Antibody

ARTICLE IN PRESS

for Hepatocellular Carcinoma. Liver Cancer. 2019;8(1):1-11.
50. Lazarov T, Juarez-Carreño S, Cox N, Geissmann F. Physiology and diseases of tissue-resident macrophages. Nature. 2023;618(7966):698-707.
51. Etzerodt A, Moulin M, Doktor TK, Delfini M, Mossadegh-Keller N, Bajenoff M, et al. Tissue-resident macrophages in omentum promote metastatic spread of ovarian cancer. J Exp Med. 2020;217(4).
52. Casanova-Acebes M, Dalla E, Leader AM, LeBerichel J, Nikolic J, Morales BM, et al. Tissue-resident macrophages provide a pro-tumorigenic niche to early NSCLC cells. Nature. 2021;595(7868):578-84.
53. Zhang QW, Liu L, Gong CY, Shi HS, Zeng YH, Wang XZ, et al. Prognostic significance of tumor-associated macrophages in solid tumor: a meta-analysis of the literature. PLoS One. 2012;7(12):e50946.
54. Gentles AJ, Newman AM, Liu CL, Bratman SV, Feng W, Kim D, et al. The prognostic landscape of genes and infiltrating immune cells across human cancers. Nat Med. 2015;21(8):938-45.
55. DeNardo DG, Ruffell B. Macrophages as regulators of tumour immunity and immunotherapy. Nat Rev Immunol. 2019;19(6):369-82.
56. Nalio Ramos R, Missolo-Koussou Y, Gerber-Ferder Y, Bromley CP, Bugatti M, Núñez NG, et al. Tissue-resident FOLR2(+) macrophages associate with CD8(+) T cell infiltration in human breast cancer. Cell. 2022;185(7):1189-207 e25.
57. Zhao J, Andreev I, Silva HM. Resident tissue macrophages: Key coordinators of tissue homeostasis beyond immunity. Sci Immunol. 2024;9(94):eadd1967.
58. Bao X, Wang D, Dai X, Liu C, Zhang H, Jin Y, et al. An immunometabolism subtyping system identifies S100A9(+) macrophage as an immune therapeutic target in colorectal cancer based on multiomics analysis. Cell Rep Med. 2023;4(4):100987.
59. Boissonnas A, Licata F, Poupel L, Jacquelin S, Fetler L, Krumeich S, et al. CD8+ tumor-infiltrating T cells are trapped in the tumor-dendritic cell network. Neoplasia. 2013;15(1):85-94.
60. Broz ML, Binnewies M, Boldajipour B, Nelson AE, Pollack JL, Erle DJ, et al. Dissecting the tumor myeloid compartment reveals rare activating antigen-presenting cells critical for T cell immunity. Cancer Cell. 2014;26(5):638-52.
61. Peranzoni E, Lemoine J, Vimeux L, Feuillet V, Barrin S, Kantari-Mimoun C, et al. Macrophages impede CD8 T cells from reaching tumor cells and limit the efficacy of anti-PD-1 treatment. Proc Natl Acad Sci U S A. 2018;115(17):E4041-E50.
62. Bao X, Li Q, Chen D, Dai X, Liu C, Tian W, et al. A multiomics analysis-assisted deep learning model identifies a macrophage-oriented module as a potential therapeutic target in colorectal cancer. Cell Rep Med. 2024;5(2):101399.
63. Kersten K, Hu KH, Combes AJ, Samad B, Harwin T, Ray A, et al. Spatiotemporal co-dependency between macrophages and exhausted CD8(+) T cells in cancer. Cancer Cell. 2022;40(6):624-38 e9.
64. Diskin B, Adam S, Cassini MF, Sanchez G, Liria M, Aykut B, et al. PD-L1 engagement on T cells promotes self-tolerance and suppression of neighboring macrophages and effector T cells in cancer. Nat Immunol. 2020;21(4):442-54.
65. Cotechini T, Atallah A, Grossman A. Tissue-Resident and Recruited Macrophages in Primary Tumor and Metastatic Microenvironments: Potential Targets in Cancer Therapy. Cells. 2021;10(4).
66. Wang C, Liu Y, Guo W, Zhu X, Ahuja N, Fu T. MAPT promoter CpG island hypermethylation is associated with poor prognosis in patients with stage II colorectal cancer. Cancer Manag Res. 2019;11:7337-43.

ARTICLE IN PRESS

ARTICLE IN PRESS

67. Pusztai L, Jeong JH, Gong Y, Ross JS, Kim C, Paik S, et al. Evaluation of microtubule-associated protein-Tau expression as a prognostic and predictive marker in the NSABP-B 28 randomized clinical trial. J Clin Oncol. 2009;27(26):4287-92.
68. Mosaad YM. Clinical Role of Human Leukocyte Antigen in Health and Disease. Scand J Immunol. 2015;82(4):283-306.
69. Iafolla MAJ, Yang C, Chandran V, Pintilie M, Li Q, Bedard PL, et al. Predicting Toxicity and Response to Pembrolizumab Through Germline Genomic HLA Class 1 Analysis. JNCI Cancer Spectr. 2021;5(1).
70. Correale P, Saladino RE, Giannarelli D, Giannicola R, Agostino R, Staropoli N, et al. Distinctive germline expression of class I human leukocyte antigen (HLA) alleles and DRB1 heterozygosis predict the outcome of patients with non-small cell lung cancer receiving PD-1/PD-L1 immune checkpoint blockade. J Immunother Cancer. 2020;8(1).
71. Yang Y, Sun J, Wang Z, Fang J, Yu Q, Han B, et al. Updated Overall Survival Data and Predictive Biomarkers of Sintilimab Plus Pemetrexed and Platinum as First-Line Treatment for Locally Advanced or Metastatic Nonsquamous NSCLC in the Phase 3 ORIENT-11 Study. J Thorac Oncol. 2021;16(12):2109-20.
72. Mei J, Jiang G, Chen Y, Xu Y, Wan Y, Chen R, et al. HLA class II molecule HLA-DRA identifies immuno-hot tumors and predicts the therapeutic response to anti-PD-1 immunotherapy in NSCLC. BMC Cancer. 2022;22(1):738.
73. Senosain MF, Zou Y, Novitskaya T, Vasiukov G, Balar AB, Rowe DJ, et al. HLA-DR cancer cells expression correlates with T cell infiltration and is enriched in lung adenocarcinoma with indolent behavior. Sci Rep. 2021;11(1):14424.
74. Gallois C, Shi Q, Meyers JP, Iveson T, Alberts SR, de Gramont A, et al. Prognostic Impact of Early Treatment and Oxaliplatin Discontinuation in Patients With Stage III Colon Cancer: An ACCENT/IDEA Pooled Analysis of 11 Adjuvant Trials. J Clin Oncol. 2023;41(4):803-15.
75. Antoniotti C, Rossini D, Pietrantonio F, Catteau A, Salvatore L, Lonardi S, et al. Upfront FOLFOXIRI plus bevacizumab with or without atezolizumab in the treatment of patients with metastatic colorectal cancer (AtezoTRIBE): a multicentre, open-label, randomised, controlled, phase 2 trial. The Lancet Oncology. 2022;23(7):876-87.
76. Lenz HJ, Parikh A, Spigel DR, Cohn AL, Yoshino T, Kochenderfer M, et al. Modified FOLFOX6 plus bevacizumab with and without nivolumab for first-line treatment of metastatic colorectal cancer: phase 2 results from the CheckMate 9X8 randomized clinical trial. J Immunother Cancer. 2024;12(3).
77. Hu H, Huang M, Li Y, Wang Z, Wang X, Liu P, et al. Perioperative chemotherapy with mFOLFOX6 or CAPOX for patients with locally advanced colon cancer (OPTICAL): A multicenter, randomized, phase 3 trial. Journal of Clinical Oncology. 2022;40(16_suppl):3500-.
78. Foxtrot Collaborative G. Feasibility of preoperative chemotherapy for locally advanced, operable colon cancer: the pilot phase of a randomised controlled trial. Lancet Oncol. 2012;13(11):1152-60.
79. Li J, Zhao X, Chen L, Guo H, Lv F, Jia K, et al. Safety and pharmacokinetics of novel selective vascular endothelial growth factor receptor-2 inhibitor YN968D1 in patients with advanced malignancies. BMC Cancer. 2010;10:529.
80. Tian S, Quan H, Xie C, Guo H, Lü F, Xu Y, et al. YN968D1 is a novel and selective inhibitor of vascular endothelial growth factor receptor-2 tyrosine kinase with potent activity in vitro and in vivo. Cancer Sci. 2011;102(7):1374-80.

ARTICLE IN PRESS

ARTICLE IN PRESS

81. Dworak O, Keilholz L, Hoffmann A. Pathological features of rectal cancer after preoperative radiochemotherapy. Int J Colorectal Dis. 1997;12(1):19-23.
82. Liu L, Liu J, Li P, Luo J, Qin R, Peng Q, et al. Single-cell analysis reveals HBV-specific PD-1(+)CD8(+) TRM cells in tumor borders are associated with HBV-related hepatic damage and fibrosis in HCC patients. J Exp Clin Cancer Res. 2023;42(1):152.
83. Fan J, Shi J, Zhang Y, Liu J, An C, Zhu H, et al. NKG2D discriminates diverse ligands through selectively mechano-regulated ligand conformational changes. EMBO J. 2022;41(2):e107739.
84. Sun X, Teng X, Liu C, Tian W, Cheng J, Hao S, et al. A Pathologically Friendly Strategy for Determining the Organ-specific Spatial Tumor Microenvironment Topology in Lung Adenocarcinoma Through the Integration of snRandom-seq and Imaging Mass Cytometry. Adv Sci (Weinh). 2024;11(26):e2308892.
85. Du J, Zhang J, Wang L, Wang X, Zhao Y, Lu J, et al. Selective oxidative protection leads to tissue topological changes orchestrated by macrophage during ulcerative colitis. Nat Commun. 2023;14(1):3675.
86. Windhager J, Zanotelli VRT, Schulz D, Meyer L, Daniel M, Bodenmiller B, et al. An end-to-end workflow for multiplexed image processing and analysis. Nat Protoc. 2023;18(11):3565-613.
87. Meier F, Brunner AD, Frank M, Ha A, Bludau I, Voytik E, et al. diaPASEF: parallel accumulation-serial fragmentation combined with data-independent acquisition. Nat Methods. 2020;17(12):1229-36.
88. Kong AT, Leprevost FV, Avtonomov DM, Mellacheruvu D, Nesvizhskii AI. MSFragger: ultrafast and comprehensive peptide identification in mass spectrometry-based proteomics. Nat Methods. 2017;14(5):513-20.
89. Yu F, Haynes SE, Teo GC, Avtonomov DM, Polasky DA, Nesvizhskii AI. Fast Quantitative Analysis of timsTOF PASEF Data with MSFragger and IonQuant. Mol Cell Proteomics. 2020;19(9):1575-85.
90. Demichev V, Messner CB, Vernardis SI, Lilley KS, Ralser M. DIA-NN: neural networks and interference correction enable deep proteome coverage in high throughput. Nat Methods. 2020;17(1):41-4.
91. Hänzelmann S, Castelo R, Guinney J. GSVA: gene set variation analysis for microarray and RNA-seq data. BMC Bioinformatics. 2013;14:7.
92. Love MI, Huber W, Anders S. Moderated estimation of fold change and dispersion for RNA-seq data with DESeq2. Genome Biol. 2014;15(12):550.
93. Yu G, Wang LG, Han Y, He QY. clusterProfiler: an R package for comparing biological themes among gene clusters. OMICS. 2012;16(5):284-7.
94. Hopewell S, Chan AW, Collins GS, Hróbjartsson A, Moher D, Schulz KF, et al. CONSORT 2025 statement: updated guideline for reporting randomised trials. BMJ. 2025;389:e081123.

Figure legends

Figure 1. (A) Overview of the study design and workflow. Paired tissue samples at baseline and during the operation were collected for cyTOF. Paired peripheral blood samples at baseline and after the end of neoadjuvant therapy were collected for cyTOF. Formalin-fixed paraffin-embedded samples at baseline were collected for IMC and spatial proteomics. (B) Trial profile. (C) Swimmer plot for clinical outcomes of patients enrolled. (D) Waterfall plot of radiological change in maximum tumour diameter from baseline. NA=not applicable, as the patient did not undergo surgery. * T3 with extramural depth ≥5 mm. (E) CT Images of 5 pCR patients before treatment (column 1) and after neoadjuvant treatments (column 2), and gross specimen of corresponding patients at the time of surgery (column 3). CT images and gross specimen showed significant tumor regression in these 5 patients after neoadjuvant therapy. pCR were confirmed by pathological examination.

ARTICLE IN PRESS

Figure 2 Global analysis of immune cell populations in tissues of CRC patients receiving neoadjuvant treatment (A) The tSNE plots of immune cells from all tissue samples, colored by different immune cell types (n=20). (B) The tSNE plots of immune cells from all tissue samples, divided into four groups based on whether they achieved pCR, before or after neoadjuvant therapy. (C) The heatmap of 11 immune cell clusters from all tissue samples. (D) Cell cluster frequency is shown as a fraction of total cells in four groups. (E) Frequency comparisons of major immune cell clusters in four groups. *p < 0.05, **p < 0.01; p-before, baseline samples for pCR patients; p-after, post-neoadjuvant therapy samples for pCR patients; n-before, baseline samples for nonpCR patients; n-after, post-neoadjuvant therapy samples for nonpCR patients.

Figure 3 The remodeling of $CD8^+$ T cell subsets after neoadjuvant therapy (A) The tSNE plots of $CD8^+$ T cells from all tissue samples, colored by five $CD8^+$ T cell subsets. (B) Pseudotime-ordered analysis of $CD8^+$ T cell clusters. (C) The heatmap of five $CD8^+$ T cell subsets. (D) Frequency of $CD8^+$ T cell subsets comparisons in four groups. *p < 0.05, **p < 0.01; p-before, baseline samples for pCR patients; p-after, post-neoadjuvant therapy samples for pCR patients; n-before, baseline samples for nonpCR patients; n-after, post-neoadjuvant therapy samples for nonpCR patients.

Figure 4 The imaging mass cytometry (IMC) reveals the spatial topology of TME at a single-cell level. (A) The workflow of IMC. (B) Single color staining of each marker. (C) Uniform Manifold Approximation and Projection (UMAP) were based on the single-cell data extracted from IMC images, showing the identified 28 distinct immune cell clusters. (D) The heatmap showing the maximum normalized mean marker expression of 28 clusters. (E) The distribution of all clusters in each ROI. (F) The percentage of each cluster of all cells visualized using boxplots. (G) The colorectal cancer tissue specimens were grouped into nonpCR and pCR based on whether they achieved pCR after treatment. The frequencies of 28 subgroups in the baseline specimens were compared between the two groups. *P < 0.05, **P < 0.01

Figure 5 Tissue neighborhood analysis reveals cell-cell interaction and communication. (A) The spatial cell interactions on IMC images. Rows represent the centered cell type and columns represent other cell types surrounding the center cell type. In each subgroup cross-box, the upper right corner represents the pCR group, and the lower left corner represents the nonpCR group. The darker (or greener) the color, the greater the number of interactions. (B) The representative ROIs of pCR and nonpCR patients. resMAC, CD8 T cells and other cells were distinguished by different colored outlines. (C) Spatial cell map and relative CN patch plots of TME. (D) Heatmaps of cell subsets corresponding to 15 CN. (E) The CN proportion between the pCR and nonpCR groups was compared. (F) Centered around resMAC, the proportional differences of surrounding immune cells between the pCR and nonpCR groups. (G) Centered around resMAC, the expression differences of the markers, including granzyme B, PD-1, PD-L1, and TIM3 for surrounding immune cells were compared between the pCR and nonpCR groups. The color of the dot represented the group with high protein expression: blue indicates high expression of the protein in the nonpCR group, while orange indicates high expression of the protein in the pCR group. The size of the dot represents the significance of the difference. *P < 0.05, **P < 0.01

Figure 6 Spatial proteomics unveiled underlying biological mechanism.
Differences in hallmark, immunotherapy-related, metabolism pathways in each patient and each condition

ARTICLE IN PRESS

revealed by unsupervised analysis ssGSEA. (B) Differentially expressed proteins between baseline samples from patients who achieved pCR and those who did not following neoadjuvant therapy. (C) The potential biological functions and relevant signaling pathways evaluated by gene ontology analysis based on significant proteins of DEPs ($P<0.05$). (D) communities of PPIs. (E) The association of cell frequencies and ssGSEA score of pathways for selected cell types by Pearson correlation coefficient.

ARTICLE IN PRESS

ARTICLE IN PRESS

Table 1 Postoperative Pathologic Findings in Patients Who Underwent Surgery (n=11)

Pathologic Finding	All patients, No. (%)	n=8 pMMR, No. (%)	n=3 dMMR, No. (%)
TRG			
TRG 0	0 (0)	0 (0)	0 (0)
TRG 1	2 (18.2)	1 (12.5)	1 (33.3)
TRG 2	1 (9.1)	1 (12.5)	0 (0)
TRG 3	3 (27.3)	2 (25.0)	1 (33.3)
TRG 4	5 (45.5)	4 (50.0)	1 (33.3)
pCR			
Yes	5 (45.5)	4 (50.0)	1 (33.3)
No	6 (54.5)	4 (50.0)	2 (66.7)
Pathologic T stage			
T0	5 (45.5)	4 (50.0)	1 (33.3)
T1	1 (9.1)	0	1 (33.3)
T2	0 (0)	0	0 (0)
T3	5 (45.5)	4 (50.0)	1 (33.3)
T4	0 (0)	0	0 (0)
Pathologic N stage			
N0	9 (81.8)	6 (75.0)	3 (100.0)
N1	2 (18.2)	2 (25.0)	0 (0)
N2	0 (0)	0 (0)	0 (0)
Distant metastasis			
M0	11 (100)	8 (100.0)	3 (100.0)
M1	0 (0)	0 (0)	0 (0)
Pathologic stage			
T0N0M0	5 (45.5)	4 (50.0)	1 (33.3)
I	1 (9.1)	0 (0)	1 (33.3)
II	3 (27.3)	2 (25.0)	1 (33.3)
III	2 (18.2)	2 (25.0)	0 (0)
IV	0 (0)	0 (0)	0 (0)
Lymphatic/vascular invasion			
Present	1 (9.1)	1 (12.5)	0 (0)
Absent	10 (90.9)	7 (87.5)	3 (100.0)
Perineural invasion			
Present	1 (9.1)	1 (12.5)	0 (0)
Absent	10 (90.9)	7 (87.5)	3 (100.0)

TRG Dworak criteria: Grade 0: no regression; Grade 1: dominant tumor mass with obvious fibrosis and/or

ARTICLE IN PRESS

vasculopathy; Grade 2: dominantly fibrotic changes with few tumor cells or groups (easy to find); Grade 3: very few (difficult to find microscopically) tumor cells in fibrotic tissue with or without mucous substance; Grade 4: no tumor cells, only fibrotic mass (total regression or response).

Table 2 Treatment-related adverse events in patients

	Grade 3-4，No. (%)	Total，No. (%)
Any TRAE	10 (83.3)	12 (100)
Hematologic		
Neutropenia	10 (83.3)	10 (83.3)
Decreased white blood cell count	4 (33.3)	8 (66.7)
Thrombocytopenia	2 (16.7)	8 (66.7)
Nonhematologic		
Hypertension	2 (16.7)	4 (33.3)
ALT increased	2 (16.7)	4 (33.3)
AST increased	0 (0)	3 (25.0)
Fatigue	0 (0)	4 (33.3)
RCCEP	0 (0)	8 (66.7)
Allergy	0 (0)	2 (16.7)
Hypothyroidism	0 (0)	2 (16.7)
Oral ulcer	0 (0)	3 (25.0)
Vomiting	0 (0)	4 (33.3)
Peripheral sensory neurotoxicity	0 (0)	4 (33.3)
Hand-foot syndrome	0 (0)	2 (16.7)

TRAE, treatment-related adverse event; RCCEP, Reactive cutaneous capillary endothelial proliferation; ALT, glutamic pyruvic transaminase; AST, glutamic oxaloacetic transaminase

ARTICLE IN PRESS

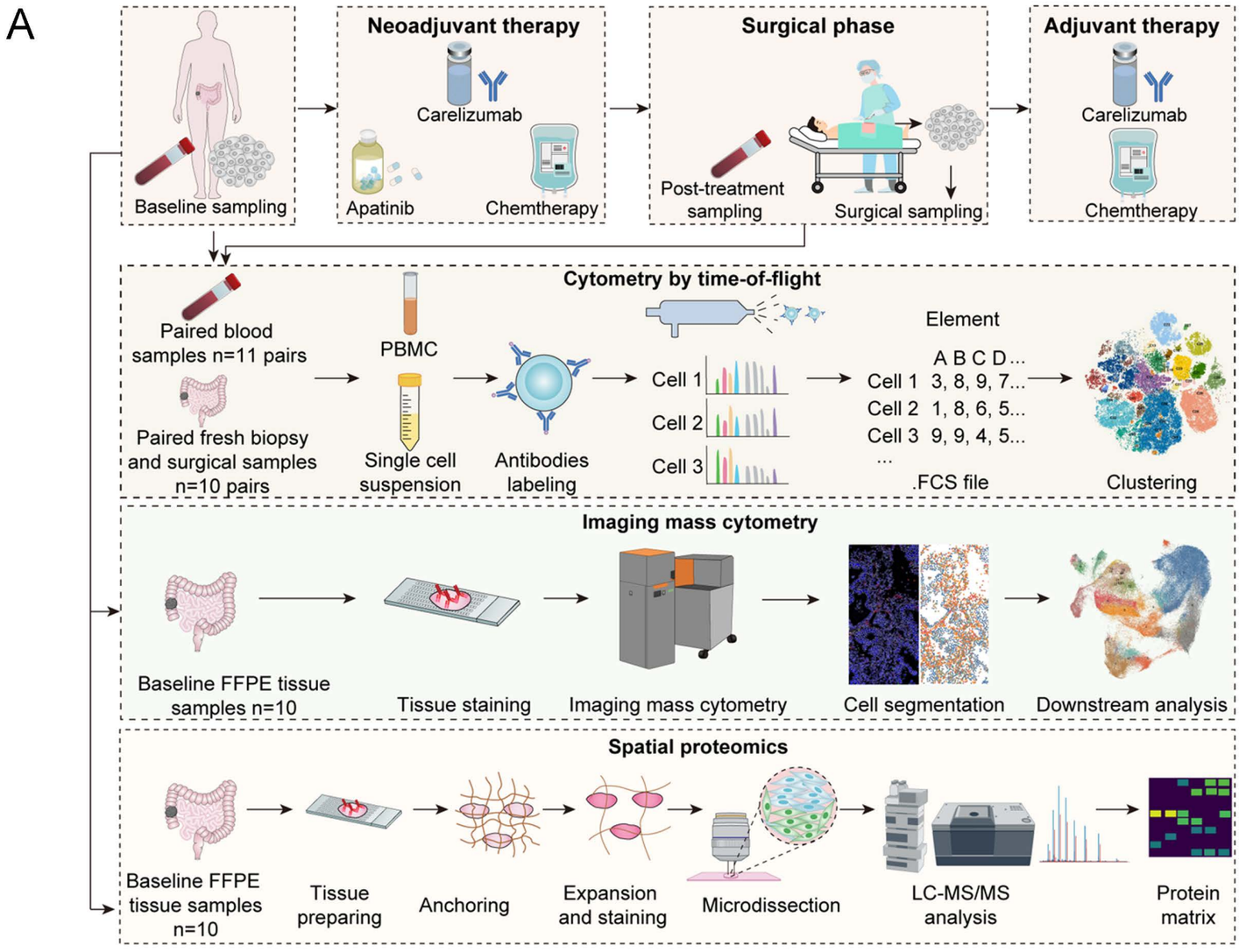
A
Baseline sampling
Neoadjuvant therapy
Carelizumab
Apatinib
Chemtherapy
Surgical phase
Post-treatment sampling
Surgical sampling
Adjuvant therapy
Carelizumab
Chemtherapy
Cytometry by time-of-flight
Paired blood samples n=11 pairs
PBMC
Paired fresh biopsy and surgical samples n=10 pairs
Single cell suspension
Antibodies labeling
Cell 1
Cell 2
Cell 3
Element
A B C D ...
Cell 1 3, 8, 9, 7...
Cell 2 1, 8, 6, 5...
Cell 3 9, 9, 4, 5...
...
.FCS file
Clustering
Imaging mass cytometry
Baseline FFPE tissue samples n=10
Tissue staining
Imaging mass cytometry
Cell segmentation
Downstream analysis
Spatial proteomics
Baseline FFPE tissue samples n=10
Tissue preparing
Anchoring
Expansion and staining
Microdissection
LC-MS/MS analysis
Protein matrix

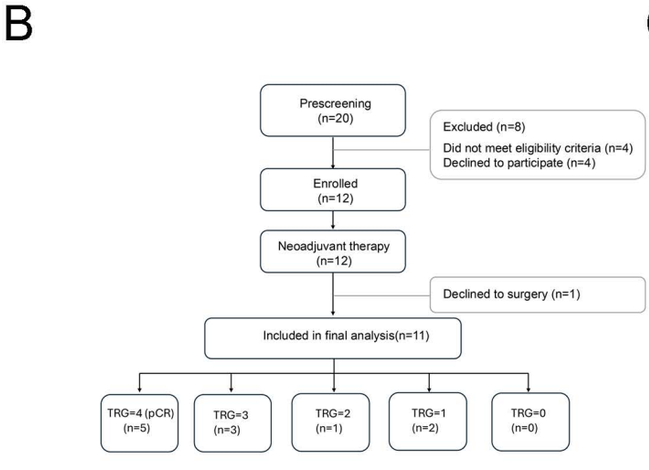
B
Prescreening (n=20)
Excluded (n=8)
Did not meet eligibility criteria (n=4)
Declined to participate (n=4)
Enrolled (n=12)
Neoadjuvant therapy (n=12)
Declined to surgery (n=1)
Included in final analysis(n=11)
TRG=4 (pCR) (n=5)
TRG=3 (n=3)
TRG=2 (n=1)
TRG=1 (n=2)
TRG=0 (n=0)

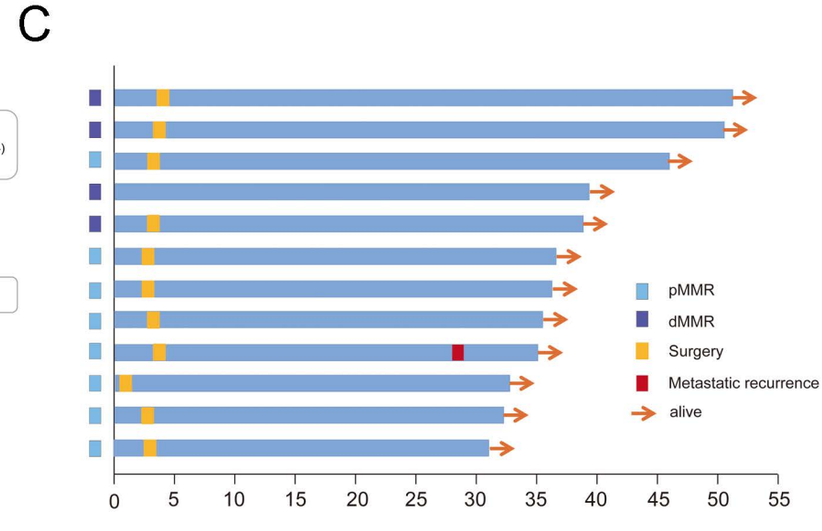
C
pMMR
dMMR
Surgery
Metastatic recurrence
alive
0
5
10
15
20
25
30
35
40
45
50
55

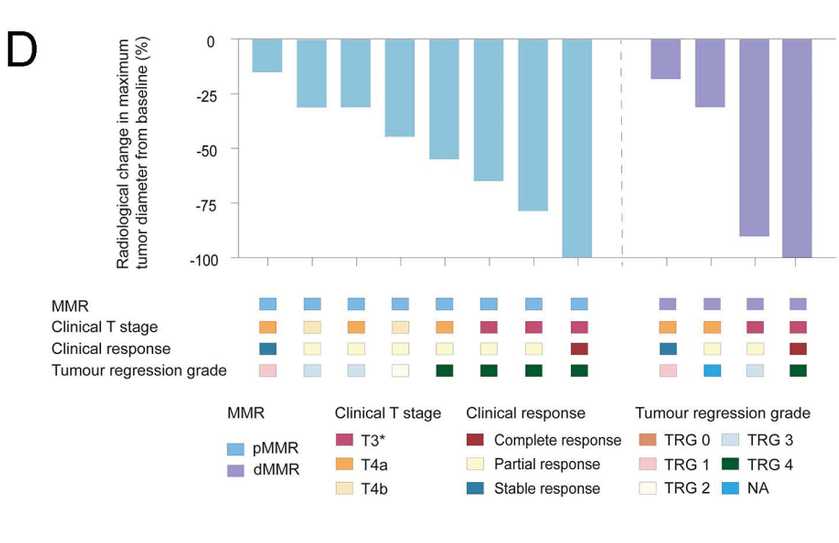
D
Radiological change in maximum tumor diameter from baseline (%)
0
-25
-50
-75
-100
MMR
Clinical T stage
Clinical response
Tumour regression grade
MMR
pMMR
dMMR
Clinical T stage
T3*
T4a
T4b
Clinical response
Complete response
Partial response
Stable response
Tumour regression grade
TRG 0
TRG 1
TRG 2
TRG 3
TRG 4
NA

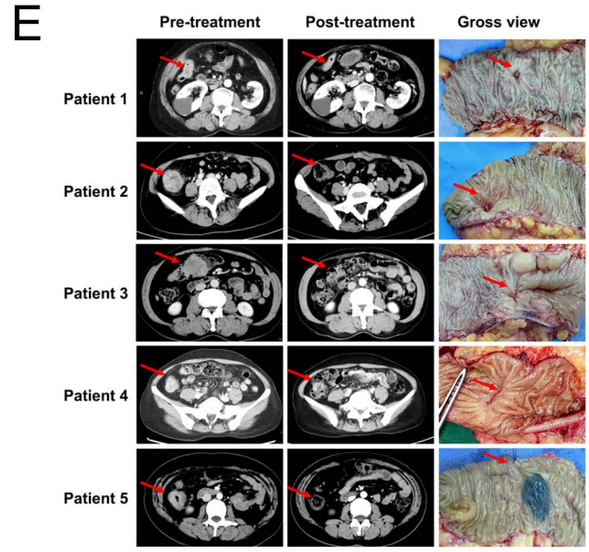
E
Pre-treatment
Post-treatment
Gross view
Patient 1
Patient 2
Patient 3
Patient 4
Patient 5

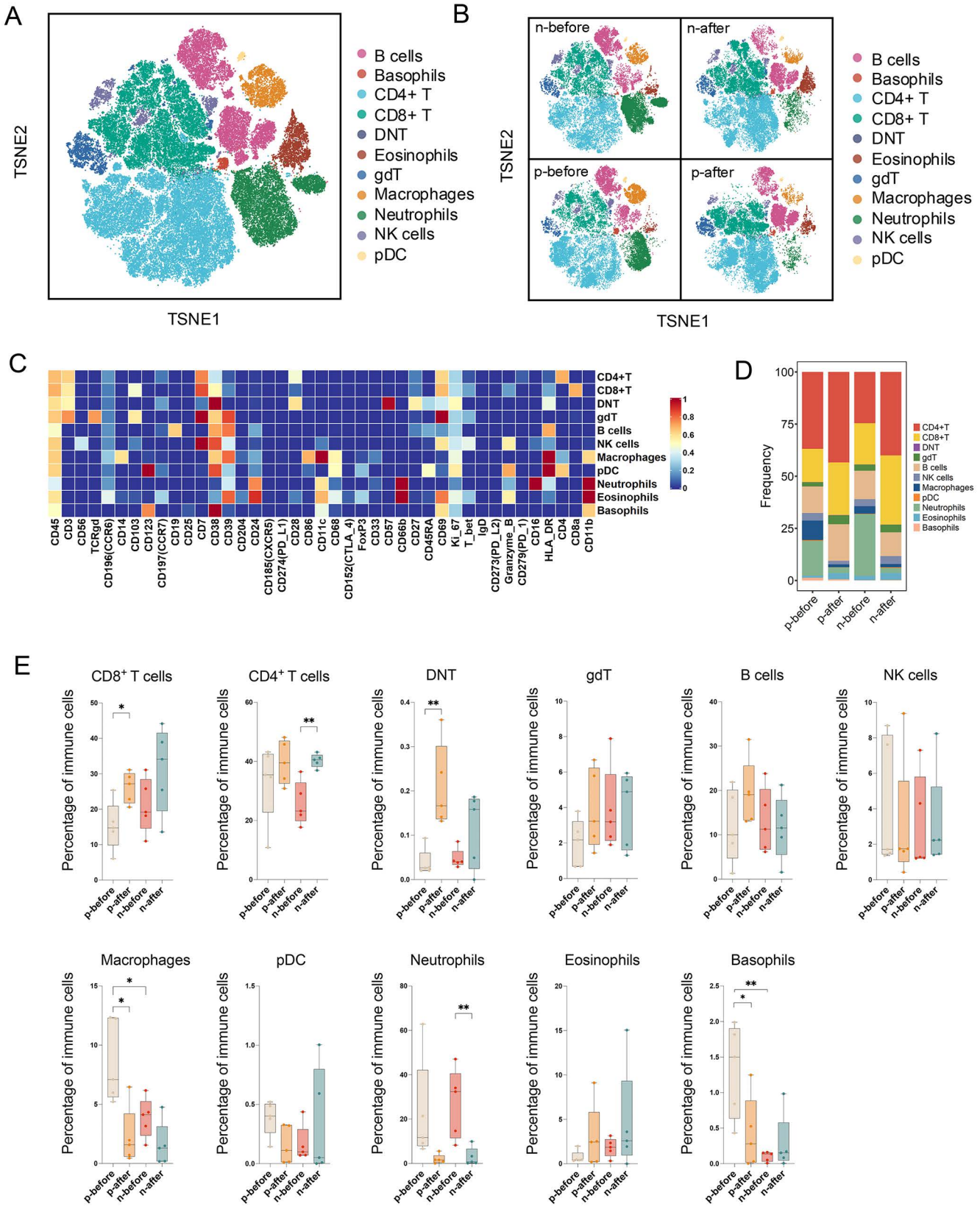
A
TSNE2
TSNE1
B cells
Basophils
CD4+ T
CD8+ T
DNT
Eosinophils
gdT
Macrophages
Neutrophils
NK cells
pDC
B
n-before
n-after
p-before
p-after
TSNE2
TSNE1
C
CD4+T
CD8+T
DNT
gdT
B cells
NK cells
Macrophages
pDC
Neutrophils
Eosinophils
Basophils
CD45 CD3 CD56 TCRgd CD196(CCR6) CD14 CD103 CD123 CD197(CCR7) CD19 CD25 CD7 CD38 CD39 CD204 CD24 CD185(CXCR5) CD274(PD_L1) CD28 CD86 CD11c CD68 CD152(CTLA_4) FoxP3 CD33 CD57 CD66b CD27 CD45RA CD69 Ki_67 T_bet IgD CD273(PD_L2) Granzyme_B CD279(PD_1) CD16 HLA_DR CD4 CD8a CD11b
1
0.8
0.6
0.4
0.2
0
D
Frequency
100
75
50
25
0
p-before
p-after
n-before
n-after
CD4+T
CD8+T
DNT
gdT
B cells
NK cells
Macrophages
pDC
Neutrophils
Eosinophils
Basophils
E
CD8+ T cells
CD4+ T cells
DNT
gdT
B cells
NK cells
Macrophages
pDC
Neutrophils
Eosinophils
Basophils
Percentage of immune cells
p-before
p-after
n-before
n-after

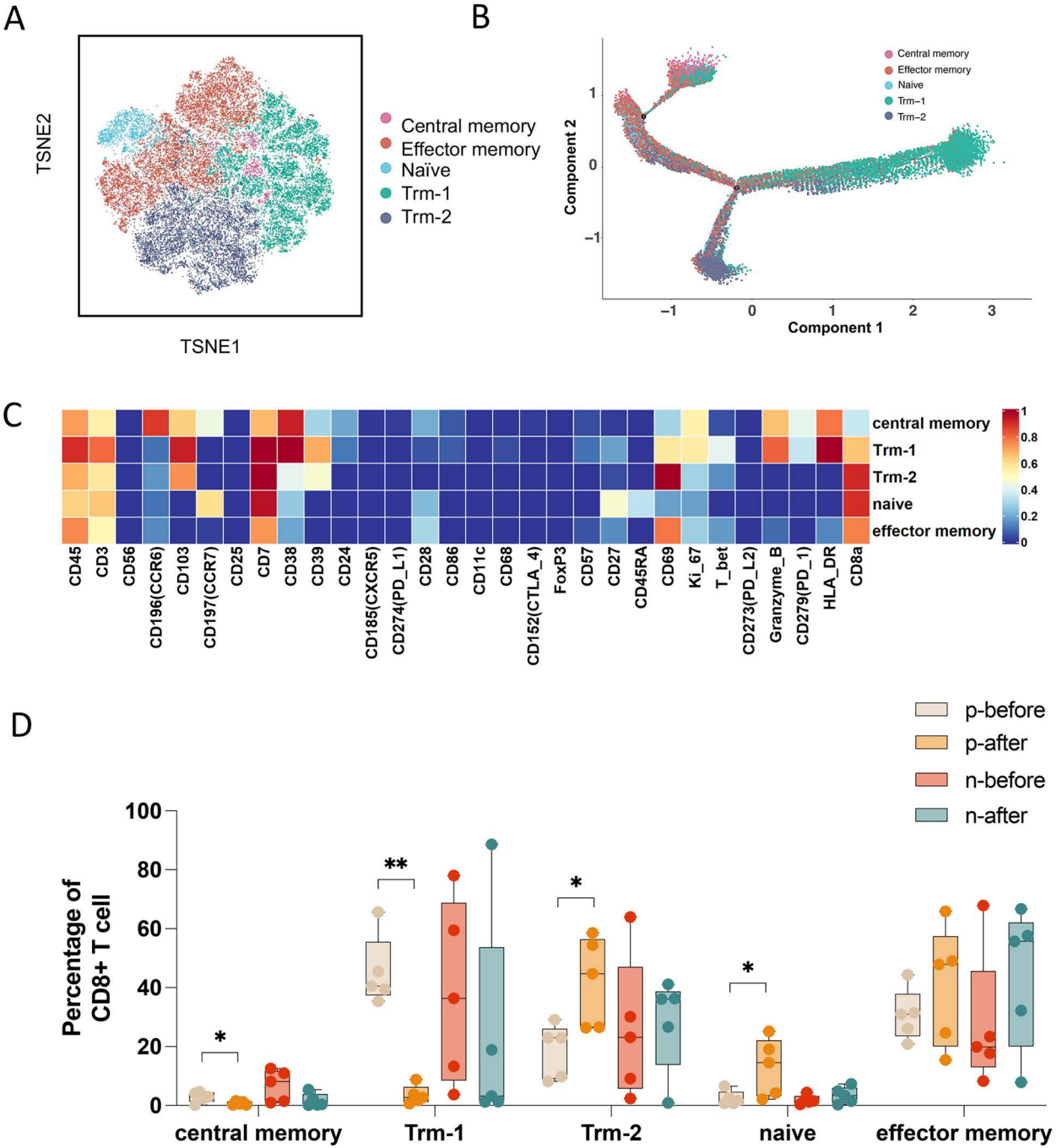
A
TSNE2
TSNE1
Central memory
Effector memory
Naïve
Trm-1
Trm-2
B
Component 2
Component 1
Central memory
Effector memory
Naive
Trm−1
Trm−2
C
central memory
Trm-1
Trm-2
naive
effector memory
CD45
CD3
CD56
CD196(CCR6)
CD103
CD197(CCR7)
CD25
CD7
CD38
CD39
CD24
CD185(CXCR5)
CD274(PD_L1)
CD28
CD86
CD11c
CD68
CD152(CTLA_4)
FoxP3
CD57
CD27
CD45RA
CD69
Ki_67
T_bet
CD273(PD_L2)
Granzyme_B
CD279(PD_1)
HLA_DR
CD8a
D
p-before
p-after
n-before
n-after
Percentage of CD8+ T cell
central memory
Trm-1
Trm-2
naive
effector memory

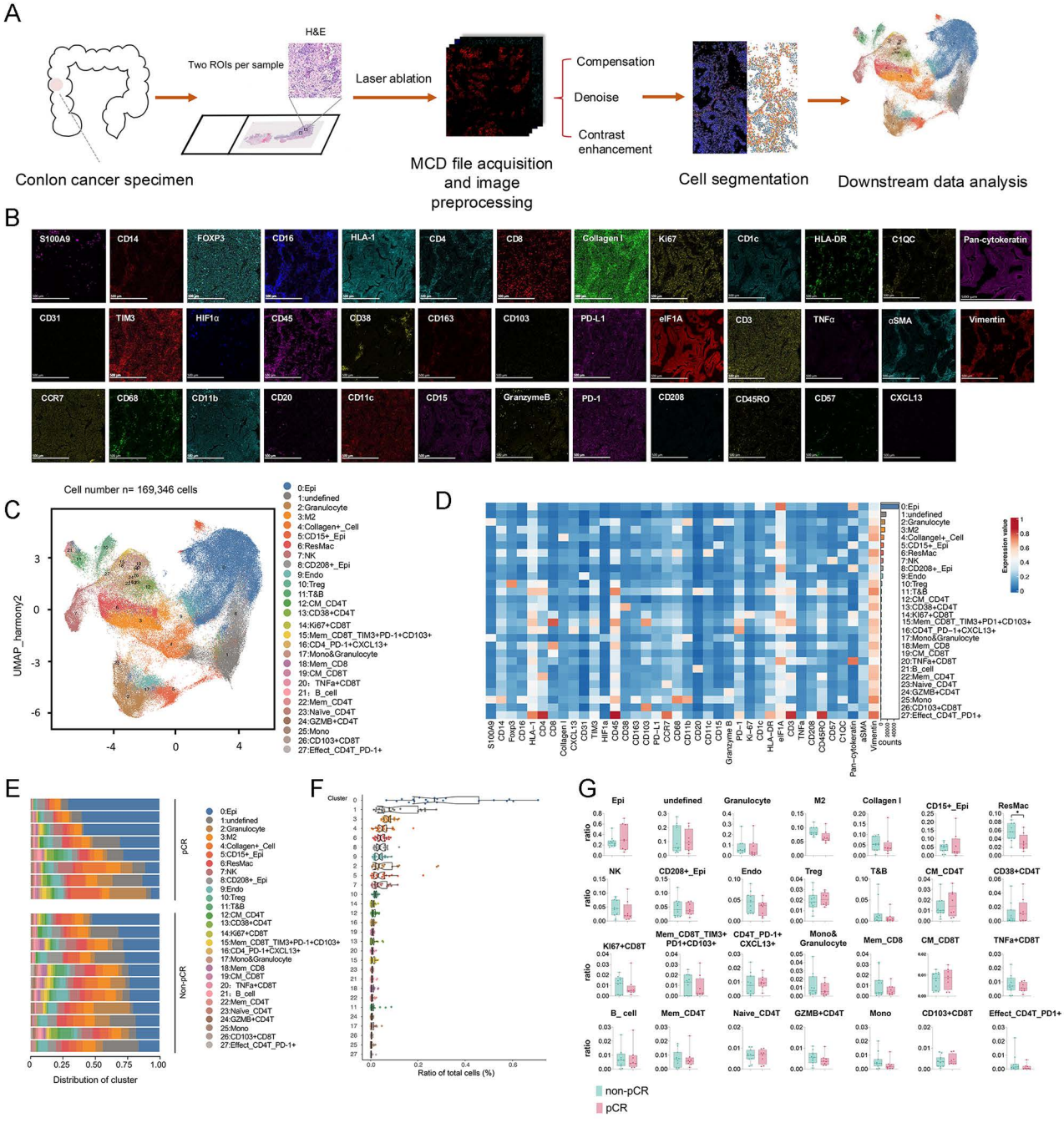
A
H&E
Two ROIs per sample
Laser ablation
Compensation
Denoise
Contrast enhancement
Conlon cancer specimen
MCD file acquisition and image preprocessing
Cell segmentation
Downstream data analysis
B
S100A9
CD14
FOXP3
CD16
HLA-1
CD4
CD8
Collagen I
Ki67
CD1c
HLA-DR
C1QC
Pan-cytokeratin
CD31
TIM3
HIF1α
CD45
CD38
CD163
CD103
PD-L1
eIF1A
CD3
TNFα
αSMA
Vimentin
CCR7
CD68
CD11b
CD20
CD11c
CD15
GranzymeB
PD-1
CD208
CD45RO
CD57
CXCL13
C
Cell number n= 169,346 cells
UMAP_harmony2
0:Epi
1:undefined
2:Granulocyte
3:M2
4:Collagen+_Cell
5:CD15+_Epi
6:ResMac
7:NK
8:CD208+_Epi
9:Endo
10:Treg
11:T&B
12:CM_CD4T
13:CD38+CD4T
14:Ki67+CD8T
15:Mem_CD8T_TIM3+PD-1+CD103+
16:CD4_PD-1+CXCL13+
17:Mono&Granulocyte
18:Mem_CD8
19:CM_CD8T
20：TNFa+CD8T
21：B_cell
22:Mem_CD4T
23:Naive_CD4T
24:GZMB+CD4T
25:Mono
26:CD103+CD8T
27:Effect_CD4T_PD-1+
D
Expression value
counts
E
pCR
Non-pCR
Distribution of cluster
F
Cluster
Ratio of total cells (%)
G
ratio
non-pCR
pCR

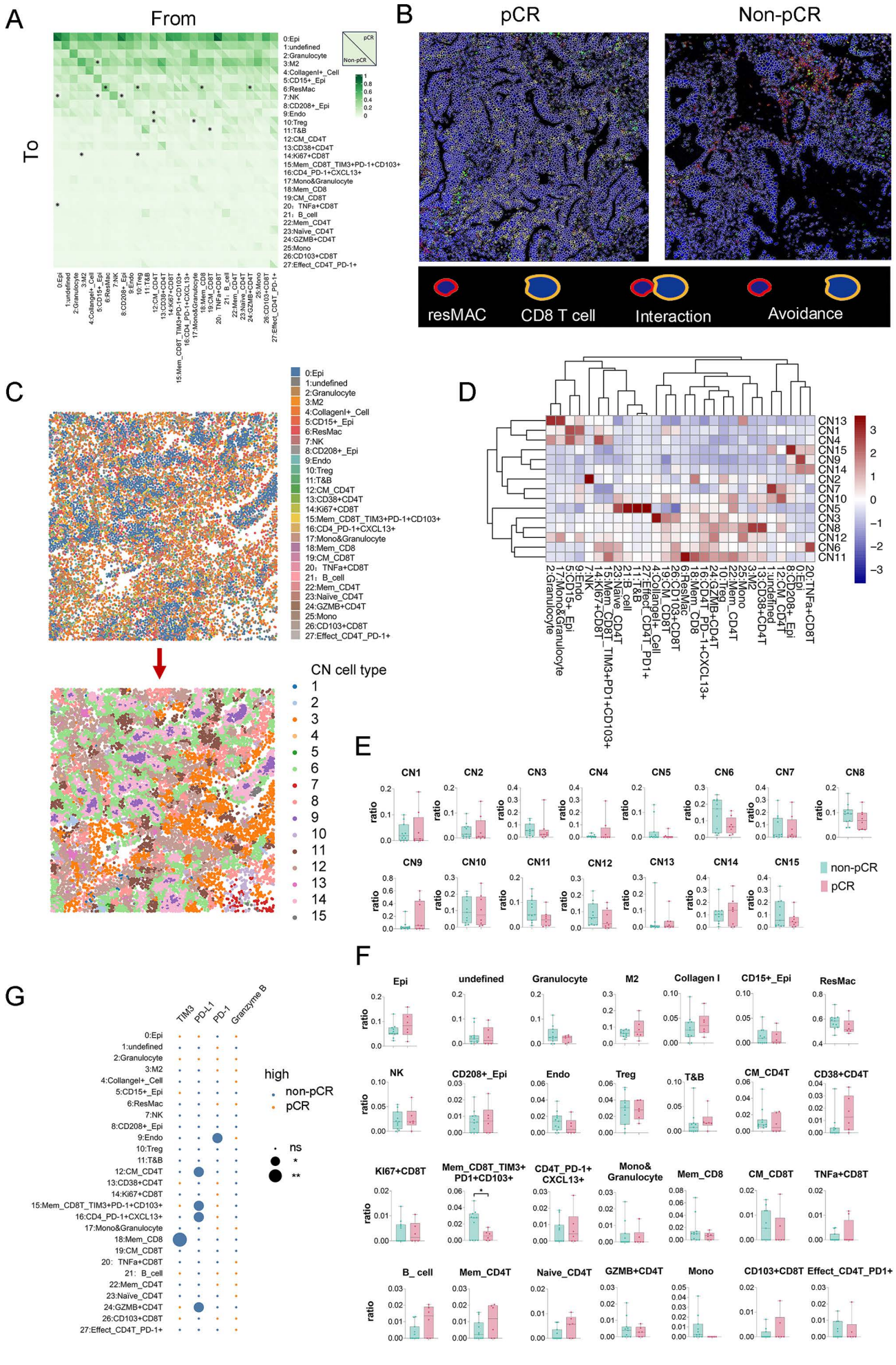
A
From
To
pCR
Non-pCR
0:Epi
1:undefined
2:Granulocyte
3:M2
4:CollagenI+_Cell
5:CD15+_Epi
6:ResMac
7:NK
8:CD208+_Epi
9:Endo
10:Treg
11:T&B
12:CM_CD4T
13:CD38+CD4T
14:Ki67+CD8T
15:Mem_CD8T_TIM3+PD-1+CD103+
16:CD4_PD-1+CXCL13+
17:Mono&Granulocyte
18:Mem_CD8
19:CM_CD8T
20：TNFa+CD8T
21：B_cell
22:Mem_CD4T
23:Naïve_CD4T
24:GZMB+CD4T
25:Mono
26:CD103+CD8T
27:Effect_CD4T_PD-1+
B
pCR
Non-pCR
resMAC
CD8 T cell
Interaction
Avoidance
C
CN cell type
D
CN13
CN1
CN4
CN15
CN9
CN14
CN2
CN7
CN10
CN5
CN3
CN8
CN12
CN6
CN11
E
CN1
CN2
CN3
CN4
CN5
CN6
CN7
CN8
CN9
CN10
CN11
CN12
CN13
CN14
CN15
ratio
non-pCR
pCR
F
Epi
undefined
Granulocyte
M2
Collagen I
CD15+_Epi
ResMac
NK
CD208+_Epi
Endo
Treg
T&B
CM_CD4T
CD38+CD4T
KI67+CD8T
Mem_CD8T_TIM3+ PD1+CD103+
CD4T_PD-1+ CXCL13+
Mono& Granulocyte
Mem_CD8
CM_CD8T
TNFa+CD8T
B_ cell
Mem_CD4T
Naive_CD4T
GZMB+CD4T
Mono
CD103+CD8T
Effect_CD4T_PD1+
G
TIM3
PD-L1
PD-1
Granzyme B
high
non-pCR
pCR
ns
*
**

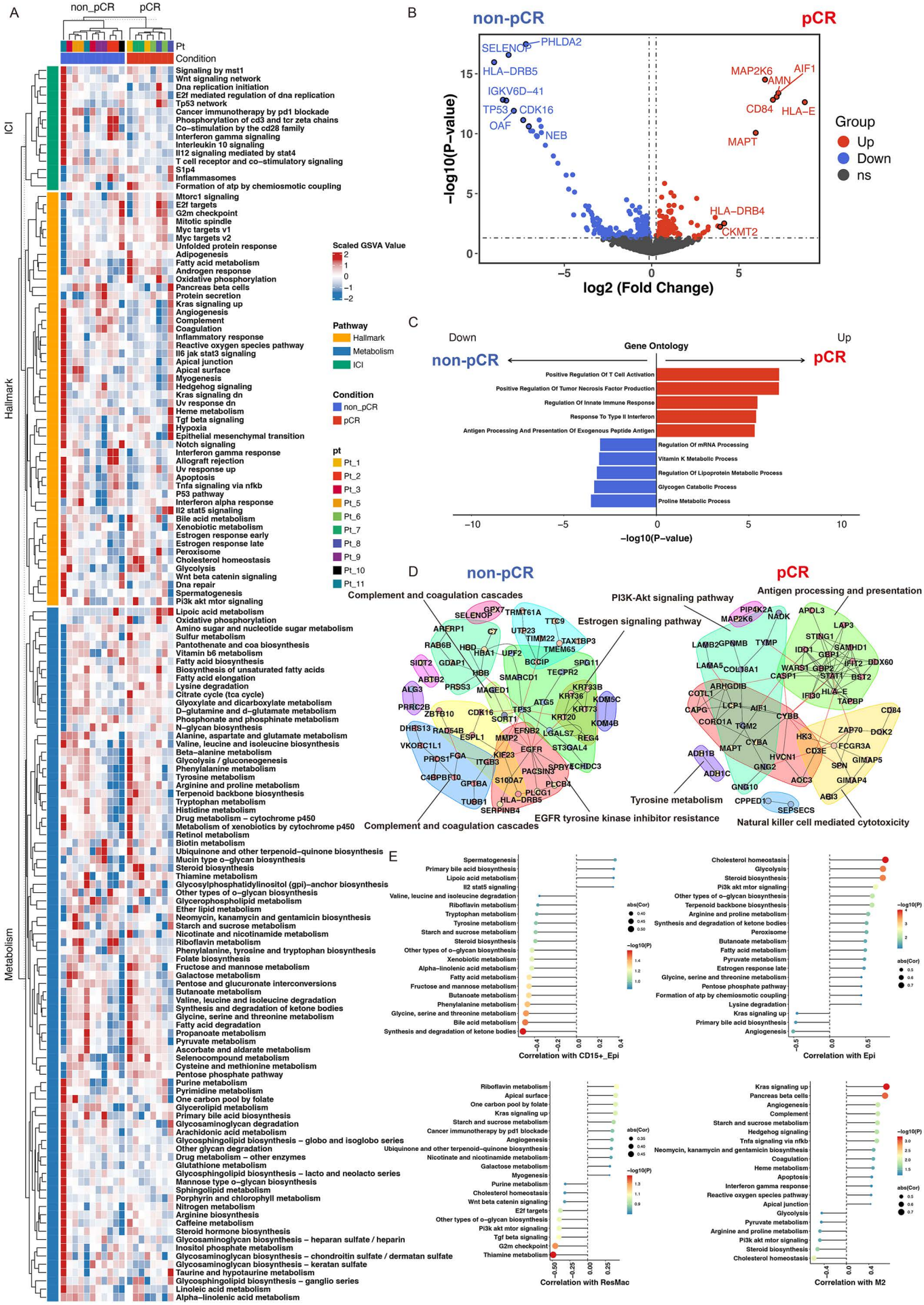
A
non_pCR
pCR
Pt
Condition
ICI
Hallmark
Metabolism
Signaling by mst1
Wnt signaling network
Dna replication initiation
E2f mediated regulation of dna replication
Tp53 network
Cancer immunotherapy by pd1 blockade
Phosphorylation of cd3 and tcr zeta chains
Co−stimulation by the cd28 family
Interferon gamma signaling
Interleukin 10 signaling
Il12 signaling mediated by stat4
T cell receptor and co−stimulatory signaling
S1p4
Inflammasomes
Formation of atp by chemiosmotic coupling
Mtorc1 signaling
E2f targets
G2m checkpoint
Mitotic spindle
Myc targets v1
Myc targets v2
Unfolded protein response
Adipogenesis
Fatty acid metabolism
Androgen response
Oxidative phosphorylation
Pancreas beta cells
Protein secretion
Kras signaling up
Angiogenesis
Complement
Coagulation
Inflammatory response
Reactive oxygen species pathway
Il6 jak stat3 signaling
Apical junction
Apical surface
Myogenesis
Hedgehog signaling
Kras signaling dn
Uv response dn
Heme metabolism
Tgf beta signaling
Hypoxia
Epithelial mesenchymal transition
Notch signaling
Interferon gamma response
Allograft rejection
Uv response up
Apoptosis
Tnfa signaling via nfkb
P53 pathway
Interferon alpha response
Il2 stat5 signaling
Bile acid metabolism
Xenobiotic metabolism
Estrogen response early
Estrogen response late
Peroxisome
Cholesterol homeostasis
Glycolysis
Wnt beta catenin signaling
Dna repair
Spermatogenesis
Pi3k akt mtor signaling
Lipoic acid metabolism
Oxidative phosphorylation
Amino sugar and nucleotide sugar metabolism
Sulfur metabolism
Pantothenate and coa biosynthesis
Vitamin b6 metabolism
Fatty acid biosynthesis
Biosynthesis of unsaturated fatty acids
Fatty acid elongation
Lysine degradation
Citrate cycle (tca cycle)
Glyoxylate and dicarboxylate metabolism
D−glutamine and d−glutamate metabolism
Phosphonate and phosphinate metabolism
N−glycan biosynthesis
Alanine, aspartate and glutamate metabolism
Valine, leucine and isoleucine biosynthesis
Beta−alanine metabolism
Glycolysis / gluconeogenesis
Phenylalanine metabolism
Tyrosine metabolism
Arginine and proline metabolism
Terpenoid backbone biosynthesis
Tryptophan metabolism
Histidine metabolism
Drug metabolism − cytochrome p450
Metabolism of xenobiotics by cytochrome p450
Retinol metabolism
Biotin metabolism
Ubiquinone and other terpenoid−quinone biosynthesis
Mucin type o−glycan biosynthesis
Steroid biosynthesis
Thiamine metabolism
Glycosylphosphatidylinositol (gpi)−anchor biosynthesis
Other types of o−glycan biosynthesis
Glycerophospholipid metabolism
Ether lipid metabolism
Neomycin, kanamycin and gentamicin biosynthesis
Starch and sucrose metabolism
Nicotinate and nicotinamide metabolism
Riboflavin metabolism
Phenylalanine, tyrosine and tryptophan biosynthesis
Folate biosynthesis
Fructose and mannose metabolism
Galactose metabolism
Pentose and glucuronate interconversions
Butanoate metabolism
Valine, leucine and isoleucine degradation
Synthesis and degradation of ketone bodies
Glycine, serine and threonine metabolism
Fatty acid degradation
Propanoate metabolism
Pyruvate metabolism
Ascorbate and aldarate metabolism
Selenocompound metabolism
Cysteine and methionine metabolism
Pentose phosphate pathway
Purine metabolism
Pyrimidine metabolism
One carbon pool by folate
Glycerolipid metabolism
Primary bile acid biosynthesis
Glycosaminoglycan degradation
Arachidonic acid metabolism
Glycosphingolipid biosynthesis − globo and isoglobo series
Other glycan degradation
Drug metabolism − other enzymes
Glutathione metabolism
Glycosphingolipid biosynthesis − lacto and neolacto series
Mannose type o−glycan biosynthesis
Sphingolipid metabolism
Porphyrin and chlorophyll metabolism
Nitrogen metabolism
Arginine biosynthesis
Caffeine metabolism
Steroid hormone biosynthesis
Glycosaminoglycan biosynthesis − heparan sulfate / heparin
Inositol phosphate metabolism
Glycosaminoglycan biosynthesis − chondroitin sulfate / dermatan sulfate
Glycosaminoglycan biosynthesis − keratan sulfate
Taurine and hypotaurine metabolism
Glycosphingolipid biosynthesis − ganglio series
Linoleic acid metabolism
Alpha−linolenic acid metabolism
Scaled GSVA Value
2
1
0
−1
−2
Pathway
Hallmark
Metabolism
ICI
Condition
non_pCR
pCR
pt
Pt_1
Pt_2
Pt_3
Pt_5
Pt_6
Pt_7
Pt_8
Pt_9
Pt_10
Pt_11
B
non-pCR
pCR
SELENOP
PHLDA2
HLA−DRB5
IGKV6D−41
TP53
CDK16
OAF
NEB
MAP2K6
AIF1
AMN
CD84
HLA−E
MAPT
HLA−DRB4
CKMT2
−log10(P−value)
log2 (Fold Change)
Group
Up
Down
ns
C
Down
Up
Gene Ontology
non-pCR
pCR
Positive Regulation Of T Cell Activation
Positive Regulation Of Tumor Necrosis Factor Production
Regulation Of Innate Immune Response
Response To Type II Interferon
Antigen Processing And Presentation Of Exogenous Peptide Antigen
Regulation Of mRNA Processing
Vitamin K Metabolic Process
Regulation Of Lipoprotein Metabolic Process
Glycogen Catabolic Process
Proline Metabolic Process
−log10(P−value)
D
non-pCR
pCR
Complement and coagulation cascades
Estrogen signaling pathway
PI3K-Akt signaling pathway
Antigen processing and presentation
Tyrosine metabolism
EGFR tyrosine kinase inhibitor resistance
Natural killer cell mediated cytotoxicity
Complement and coagulation cascades
E
Correlation with CD15+_Epi
Correlation with Epi
Correlation with ResMac
Correlation with M2
abs(Cor)
−log10(P)